

Infrared identification of hard X-ray sources in the Galaxy

A. Nebot Gómez-Morán,^{1★} C. Motch,¹ F.-X. Pineau,¹ F. J. Carrera,² M. W. Pakull¹ and F. Riddick³

¹Observatoire Astronomique de Strasbourg, Université de Strasbourg, CNRS, UMR 7550, 11 rue de l'Université, F-67000 Strasbourg, France

²Instituto de Física de Cantabria (CSIC-UC), Avenida de los Castros, E-39005 Santander, Spain

³Isaac Newton Group of Telescopes, Apartado de Correos 321, E-38700 Santa Cruz de La Palma, Spain

Accepted 2015 May 6. Received 2015 April 24; in original form 2014 October 6

ABSTRACT

The nature of the low- to intermediate-luminosity ($L_X \sim 10^{32-34} \text{ erg s}^{-1}$) source population revealed in hard band (2–10 keV) X-ray surveys of the Galactic plane is poorly understood. To overcome such problem, we cross-correlated the *XMM-Newton* 3XMM-DR4 survey with the infrared Two Micron All Sky Survey and Galactic Legacy Infrared Mid-Plane Survey Extraordinaire catalogues. We identified reliable X-ray–infrared associations for 690 sources. We selected 173 sources having hard X-ray spectra, typical of hard X-ray high-mass stars ($kT > 5 \text{ keV}$), and 517 sources having soft X-ray spectra, typical of active coronae. About 18 per cent of the soft sources are classified in the literature: ~ 91 per cent as stars, with a minor fraction of Wolf–Rayet (WR) stars. Roughly 15 per cent of the hard sources are classified in the literature: ~ 68 per cent as high-mass X-ray stars single or in binary systems (WR, Be and high-mass X-ray binaries – HMXBs), with a small fraction of G and B stars. We carried out infrared spectroscopic pilot observations at the William Herschel Telescope for five hard X-ray sources. Three of them are high-mass stars with spectral types WN7-8h, Ofpe/WN9 and Be, and $L_X \sim 10^{32-10^{33}} \text{ erg s}^{-1}$. One source is a colliding-wind binary, while another source is a colliding-wind binary or a supergiant fast X-ray transient in quiescence. The Be star is a likely γ -Cas system. The nature of the other two X-ray sources is uncertain. The distribution of hard X-ray sources in the parameter space made of X-ray hardness ratio, infrared colours and X-ray-to-infrared flux ratio suggests that many of the unidentified sources are new γ -Cas analogues, WRs and low L_X HMXBs. However, the nature of the X-ray population with $K_s \geq 11$ and average X-ray-to-infrared flux ratio remains unconstrained.

Key words: stars: emission-line, Be – stars: Wolf–Rayet – X-rays: binaries – X-rays: stars.

1 INTRODUCTION

The landscape of the Galaxy is dominated by relatively nearby stellar coronae at low X-ray luminosities ($L_X < 10^{31} \text{ erg s}^{-1}$) and soft energies ($< 2 \text{ keV}$; e.g. Motch et al. 1997; Nebot Gómez-Morán et al. 2013). In contrast, at high X-ray luminosities ($L_X > 10^{35} \text{ erg s}^{-1}$), the make-up of the Milky Way is dominated by high-mass X-ray binaries (HMXBs; Grimm, Gilfanov & Sunyaev 2002; Gilfanov 2004) and low-mass X-ray binaries (LMXB; Grimm, Gilfanov & Sunyaev 2002; Gilfanov 2004). On the other hand, the nature of the low- to intermediate-luminosity source population revealed in hard band (2–10 keV) X-ray surveys of the Galactic plane, such as those carried out by ASCA (Sugizaki et al. 2001) and more recently by *Chandra* (e.g. Ebisawa et al. 2005) and *XMM-Newton* (e.g. Hands

et al. 2004) is only partly understood. Importantly, in this L_X range we expect to find systems predicted by evolutionary scenarios of LMXBs and HMXBs. For instance, we have not yet detected the long-lived wind-accreting low X-ray luminosity stages preceding or following the bright phase during which they become conspicuous. The common envelope spiral-in creation channel for LMXBs predicts the existence of pre-LMXBs which could radiate as much as $\sim 10^{32} \text{ erg s}^{-1}$ in hard X-rays through accretion of stellar wind on to the neutron star or its magnetosphere (see e.g. Tauris & van den Heuvel 2006). Likewise, evolution theories of HMXBs foresee that about 10^6 wind accreting binaries containing a main-sequence star and a neutron star or a black hole populate the Galaxy (Pfahl, Rappaport & Podsiadlowski 2002). Moreover, Be + white dwarf systems are expected to be 10 times more frequent than Be + neutron stars binaries (Raguzova 2001), whereas none is known so far in our Galaxy. With mass accretion rates potentially similar to cataclysmic variables (CVs), many of these systems should emit

* E-mail: ada.nebot@astro.unistra.fr

copious amounts of hard X-rays. A census of the contribution of the different populations to the Galactic hard X-ray emission is hence needed if we want to test the validity of these evolutionary models.

Active binaries such as RS CVn systems, and CVs are expected to contribute significantly to the low-luminosity hard X-ray source population (Sazonov et al. 2006; Revnivtsev et al. 2009). Massive objects such as magnetic OB stars (Gagné et al. 2011), colliding-wind binary O or Wolf–Rayet (WR) stars (Mauerhan et al. 2010; Skinner et al. 2010), γ -Cas like objects, being so far the best Be + WD candidates (Motch et al. 2007), and X-ray transient binaries in quiescent state have also been identified in this luminosity range. However, despite significant efforts (Motch et al. 2010; Anderson et al. 2011), our knowledge of the makeup of the Galactic low- to medium-luminosity hard X-ray source population associated with massive stars is restricted due to the lack of fully identified X-ray source samples. First, the space density of each of these subclasses of X-ray sources is basically unconstrained and, secondly, it remains to be seen whether any new types of Galactic X-ray-emitting massive stars, such as those predicted by evolutionary theories (e.g. Be + white dwarf systems), are present within current hard X-ray Galactic surveys. Owing to sensitivity limits and localization accuracies such studies can only be carried out in our Galaxy.

In this paper, we investigate the properties of this important class of massive X-ray sources of low- to intermediate-luminosity by observing candidates selected from the most recent X-ray and infrared surveys. Our target selection, based on the cross-correlation of the 3XMM-DR4 catalogue with the Two Micron All Sky Survey (2MASS) and Galactic Legacy Infrared Mid-Plane Survey Extraordinaire (GLIMPSE) catalogues, is described in Section 2. As part of a pilot study, we obtained infrared spectroscopic observations of a small sample of hard X-ray sources (see Section 3), and produced images of the target environment (see Section 4), which helped to classify the sources (see Section 5). We discuss our results in Section 6 and conclude in Section 7.

2 TARGET SELECTION

In this section, we briefly describe the cross-matched catalogues and the cross-matching procedure. We explain our selection criterion and list the X-ray sources chosen for further study at the telescope.

2.1 Cross-matched catalogues

2.1.1 3XMM-DR4

ESA's X-ray Multi-Mirror observatory *XMM-Newton* was launched in 1999 December, and started operations at the beginning of 2000 (Jansen et al. 2001). It has three telescopes, each equipped with one X-ray CCD camera, comprising the European Photon Imaging Camera (EPIC). Two of the cameras are MOS CCD detectors (referred to as MOS-1 and MOS-2 cameras; Turner et al. 2001) and the third is a pn CCD detector (referred to as EPIC-pn camera; Strüder et al. 2001). While the EPIC-pn camera receives all the incident light, a grating disperses about 40 per cent of the light going to the EPIC-MOS cameras, diverging it to two Reflection Grating Spectrometers (RGS; den Herder et al. 2001). The field of view (FOV) of the telescope is about 30 arcmin diameter and the EPIC cameras are sensitive in the energy range 0.2–12 keV with a spectral resolution $E/\Delta E$ of about 20–50 and a spatial resolution of 5 arcsec (full width at half-maximum). The *XMM-Newton* Survey Science Centre (SSC) compiles catalogues of serendipitous sources

detected by the EPIC cameras on board the *XMM-Newton* satellite (Watson et al. 2009). The 3XMM-DR4 catalogue was released on the 2013 September 15¹ and contains 531 261 detections for 372 728 unique X-ray sources. Taking into account overlaps the sky coverage is 794 deg², about 1.4 per cent of the sky. The limiting X-ray flux in the 0.2–12 keV band is $\sim 2 \times 10^{-15}$ erg cm⁻² s⁻¹ and source positions have a typical accuracy better than 3 arcsec (90 per cent confidence radius). Among other parameters, the catalogue contains information on the count rate, some flags describing the quality of the observation, the extension of the source, and the hardness ratios (HR), X-ray colours defined as

$$\text{HR}_i = \frac{C_{i+1} - C_i}{C_{i+1} + C_i}, \quad (1)$$

where C_i stands for the count rate in the energy band i , where $i = 0.2\text{--}0.5, 0.5\text{--}1.0, 1.0\text{--}2.0, 2.0\text{--}4.5, 4.5\text{--}12.0$ keV.

2.1.2 GLIMPSE

The GLIMPSE (Benjamin et al. 2003) is a *Spitzer* Space Telescope Mission programme that aims to map the inner regions of the Galaxy in the infrared. GLIMPSE source catalogue (I, II + 3D) was published in 2009 June (Spitzer Science 2009) through VizieR (Ochsenbein, Bauer & Marcout 2000). It provides images and magnitudes for over 104 million sources in four bands: 3.6, 4.5, 5.8, and 8.0 μm (I1, I2, I3 and I4). The catalogue covers Galactic longitudes $\pm 65^\circ$ and latitudes $\pm 1^\circ$ (up to $\pm 3^\circ$ in the inner regions of the Galaxy). Spatial resolution is < 2 arcsec, and magnitude limits are about 15.5, 15.0, 13.0, and 13.0 in each band, respectively (Churchwell et al. 2009). GLIMPSE covers about 1 per cent of the sky with a typical position accuracy of 0.3 arcsec.

2.1.3 2MASS PSC

The 2MASS (Skrutskie et al. 2006) used two 1.3 m telescopes located in the northern and southern hemispheres equipped with near-infrared cameras to obtain simultaneous photometry in three bands: J (1.25 μm), H (1.65 μm) and K_s (2.17 μm), for the entire sky. The 2MASS point source catalogue was released in 2003 and contains about 471 million sources. The angular resolution is 2 arcsec and the survey completeness limits are $J = 15.8$, $H = 15.1$ and $K_s = 14.3$ mag. The mean position accuracy is ~ 80 mas rms (Cutri et al. 2003).

2.2 Cross-match procedure

We cross-matched the 3XMM-DR4 catalogue with the 2MASS and GLIMPSE catalogues using the method developed by Pineau et al. (2011). In brief, this method looks for all the catalogue sources around the X-ray source position within a distance lower than $3.439\sigma_{\text{XC}}$, corresponding to a completeness of 99.7 per cent. Here, σ_{XC} is the combined positional error of the two catalogues that are being cross-matched added in quadrature. For all the matches found within this distance, i.e. for all infrared candidates associated with a X-ray source, the method computes the likelihood ratio (LR) between the probability that the two sources (X-ray and infrared sources) are associated (P_{id}) and thus have the same position, and the probability of finding a spurious association at the same angular

¹ http://xmmssc-www.star.le.ac.uk/Catalogue/3XMM-DR4/UserGuide_xmmcat.html

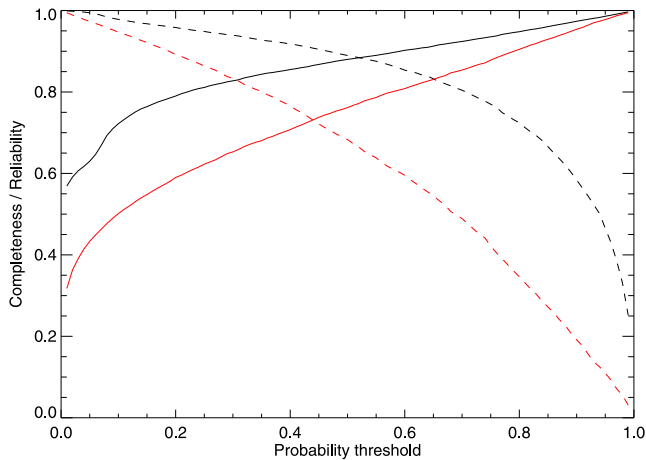


Figure 1. Completeness (dashed line) and reliability (solid line) of the 3XMM-2MASS and 3XMM-GLIMPSE associations as a function of the threshold in the probability is shown in black and red, respectively.

Table 1. Completeness and spurious fraction of X-ray-infrared associations.

		3XMM-2MASS P_{id}^a				
		50%	60%	70%	80%	90%
Completeness		89%	85%	80%	72%	58%
spurious fr.		12%	10%	8%	6%	3%
		3XMM-GLIMPSE P_{id}				
		50%	60%	70%	80%	90%
Completeness		68%	59%	49%	35%	19%
spurious fr.		24%	19%	15%	10%	5%

Notes. ^aLimited to the GLIMPSE footprint.

distance and with the same magnitude or brighter than the candidate. For that purpose, local densities are calculated for sources brighter than the candidate. The LR depends on the probability of an X-ray source to have a counterpart in the considered catalogue, which depends on the object type considered, its properties and the relative fractions of the different populations. To estimate P_{id} , it is common to build LR histograms and determine the contribution of spurious associations through time-consuming Monte Carlo simulations where positions and errors are randomized. In the method developed by Pineau et al. (2011), the number of spurious associations in each LR bin is estimated, assuming a mean local surface density of X-ray sources, as the sum over all possible associations of the ratio between the surface element (convolution ellipse defined by the positions and their errors) and the FOV area. Once the rate of spurious associations is calculated P_{id} can be estimated for each LR bin.

For sources above a given threshold in the identification probability, the method provides us with the completeness and the fraction of possible spurious associations in the cross-matched survey (see Fig. 1). In Table 1, we list the survey completeness and the fraction of spurious catalogue identifications as a function of P_{id} . In practice, we excluded sources uncorrected for satellite attitude errors (task EPOSCOR) and with positional errors (SC_POSERR) in the 3XMM-DR4 catalogue larger than 5 arcsec. For the GLIMPSE catalogue, we took into account all sources from the v2.0 Archive (v2.0_GLMIIA), i.e. sources detected twice in at least one band with $S/N > 5$ and we limited our sample to sources brighter than 14 mag in the 4.5 μm band, corresponding to a catalogue complete-

ness of 90 per cent (Kobulnicky et al. 2013). For the 2MASS-PSC catalogue, we only considered sources with the best photometric quality, $Q_{flag} = \text{'AAA'}$, which corresponds to an $S/N > 10$ and brighter than 15.8 mag in the J band, level at which the catalogue is 99 per cent complete.² We only cross-matched the 3XMM-DR4 and the 2MASS catalogues in areas also covered by GLIMPSE.

To speed up the process, we made use of HEALPix Multi Order Coverage maps (MOC)³ which provided us with the coverage of a survey within a given minimum pixel resolution. Before performing the cross-match, we pre-selected *XMM-Newton* sources within the footprint of the GLIMPSE survey. We accessed corresponding MOCs from the interactive software sky atlas ALADIN (Bonnarel et al. 2000), and selected sources within the MOC making use of the function *inMoc* in TOPCAT⁴ (Taylor 2011). The overlap between 3XMM-DR4 and GLIMPSE footprints covers 0.1 per cent of the sky, and contains 31 115 unique X-ray sources.

We found 15 018 possible 3XMM-2MASS pairs (for 9437 unique 3XMM sources) and 56 751 3XMM-GLIMPSE possible pairs (for 16 668 unique 3XMM sources). In the left-hand panel of Fig. 2, we show magnitude histograms of all the possible pairs above a certain associated probability. The higher the cut in P_{id} the brighter the subsample is, implying that we can only find reliable X-ray-infrared associations, i.e. a small fraction of spurious associations, for relatively bright infrared sources.

2.2.1 3XMM, 2MASS, GLIMPSE associations

Once all the possible 3XMM-2MASS and 3XMM-GLIMPSE associations were obtained, the next step was to identify each 3XMM-2MASS-GLIMPSE unique association. For that purpose, we proceeded as follows.

We limited the sample to X-ray good quality point-like sources above a 4σ detection. For assuring a 4σ detection, we selected sources with parameter $sc_det_ml > 10$. We defined sources as good X-ray detections if $sum_flag \leq 2$, where sum_flag contains the summary information on 12 flags set automatically and manually which indicate the quality of the X-ray detection. We restricted our sample to point-like X-ray sources, for which we imposed $SC_EXTENT = 0$, i.e. no additional source extent model was convolved with the point spread function fit to the source count distribution.

We restricted our study to associations with 3XMM-2MASS $P_{id} > 0.6$, value at which the expected fraction of spurious associations is about 10 per cent (see Table 1). For each of these unique 3XMM-2MASS associations, we looked for all possible 3XMM-GLIMPSE counterparts, based on their unique 3XMM-IAUNAME identifier, and we considered the right match the one with the highest 3XMM-GLIMPSE P_{id} . In this way, we found 2988 possible 3XMM-2MASS-GLIMPSE associations. Being aware that this could eventually lead to wrong associations we created finding charts and visually inspected them to ensure that the chosen GLIMPSE counterpart is the correct one. In the right-hand panel of Fig. 2, we plot the distance between 3XMM-2MASS and the 3XMM-GLIMPSE pairs. There are a few cases where the distance to the 2MASS association is clearly larger than that of the GLIMPSE association and vice versa. Visual inspection in these cases revealed that the 2MASS and GLIMPSE sources are possibly not associated.

² http://www.ipac.caltech.edu/2mass/releases/allsky/doc/sec2_2.html

³ <http://www.ivoa.net/documents/MOC/index.html>

⁴ <http://www.star.bris.ac.uk/mbt/topcat/>

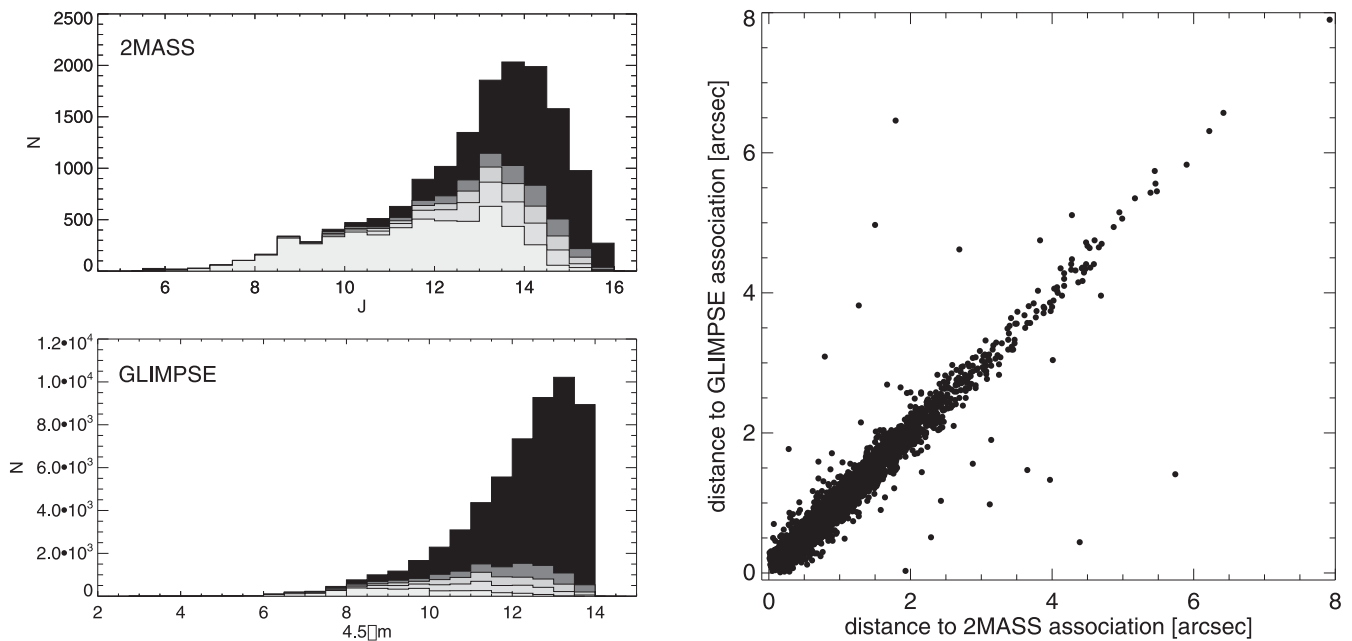


Figure 2. Left-hand panel: number of possible 3XMM-2MASS (top) and 3XMM-GLIMPSE (bottom) associations per magnitude bin for $P_{id} > 0.2, 0.4, 0.6, 0.8,$ and 1 (black, dark grey, grey, medium grey and light grey, respectively). Right-hand panel: distance between the 3XMM-GLIMPSE possible associations against the 3XMM-2MASS associations for pairs with a common 3XMM source.

We prefer to be cautious about these cases and flag them as dubious for any further study. We also checked whether our associations between 2MASS and GLIMPSE sources were in agreement with those given in the GLIMPSE catalogue. In 10 cases, we had different associations and in another 29 cases no association was given in the GLIMPSE catalogue. All these 39 cases corresponded to associations already flagged as being dubious based on visual inspection of their finding charts. We calculated the distance between 2MASS and GLIMPSE sources and found that most of the 3XMM-2MASS-GLIMPSE associations with high P_{id} have a distance smaller than 1 arcsec.

2.3 Selection of hard X-ray high-mass star candidates

To distinguish sources that are likely active coronae with soft X-ray spectra from high-mass stars with hard X-ray spectra we compared the observed X-ray properties of our sample with modelled data. Following the same approach as in Nebot Gómez-Morán et al. (2013), we modelled X-ray spectra for different types of objects:

(i) Model 1: a young population (70 Myr) of active coronae, for which we assumed two temperature thermal emission components, one component ($kT_1 = 0.5$ keV) representing the hot plasma and a second hotter component ($kT_2 = 0.8$ keV; Güdel, Guinan & Skinner 1997).

(ii) Model 2: RS CVn binaries, for which we took as a model values of WW Dra (Dempsey et al. 1993), with $(kT_1, kT_2) = (0.2, 2.1)$ and emissivities $EM_2/EM_1 = 0.67$.

(iii) Model 3: a population of hard X-ray massive stars. We chose one single temperature plasma $kT = 5$ keV as a representative value of a population of hard X-ray massive stars containing WR stars (see e.g. WR 142; Oskinova et al. 2009; Sokal et al. 2010) and γ -Cas analogues (Lopes de Oliveira 2007).

We modelled the emission of these three different populations as a function of Galactic absorption and we computed the corresponding

HR. For more details, we refer the reader to Nebot Gómez-Morán et al. (2013).

Among the 3XMM-2MASS-GLIMPSE associations, a large fraction have rather large HR errors, making it difficult to differentiate between soft and hard sources. To avoid such problem, we only considered sources in our sample with errors smaller than 0.2 in HR3 and HR4, a value close to the mean error in the 3XMM-DR4 catalogue. We finally restricted the sample to sources with errors in the HR2 smaller than 1 and that have been detected in the EPIC-pn camera, so as to compute fluxes avoiding any possible problems related to the merging of the EPIC-MOS and EPIC-pn individual detections. We preferred the EPIC-pn camera due to its higher sensitivity compared to the two EPIC-MOS cameras. After applying these cuts, we were left with 690 3XMM-2MASS-GLIMPSE unique associations.⁵

In Fig. 3, we show the location of all the 690 sources in two HR versus $(H - K_s)$ diagrams. Since the colour $(H - K_s)$ remains within 0 to +0.1 from A to K spectral types, independent on the luminosity class (Covey et al. 2007), variations in colour mainly reflect variations in Galactic absorption or intrinsic emission by circumstellar matter. Under the assumption of no intrinsic colour, i.e. $(H - K_s) = 0$, we calculated the expected HR as a function of $(H - K_s)$, using the formula $N_H = 3.5 \times 10^{22} \times E(H - K_s)$, for the different kind of objects for which we modelled the X-ray spectra. We compared the observed values to modelled values for active corona, RS CVn binaries and hard X-ray massive stars. Among these three type of objects, only hard X-ray massive stars

⁵ Associations 3XMM J174505.4–285117–2MASS 17450537–2851166–G000.0088+00.1411, 3XMM J175703.9–295921–2MASS 17570406–2959219–G000.3666–02.6797 and 3XMM J174912.4–272537–2MASS 17491250–2725357–G001.7001+00.1051 are dubious, the distance between the 2MASS and the GLIMPSE possible counterparts is larger than 1 arcsec.

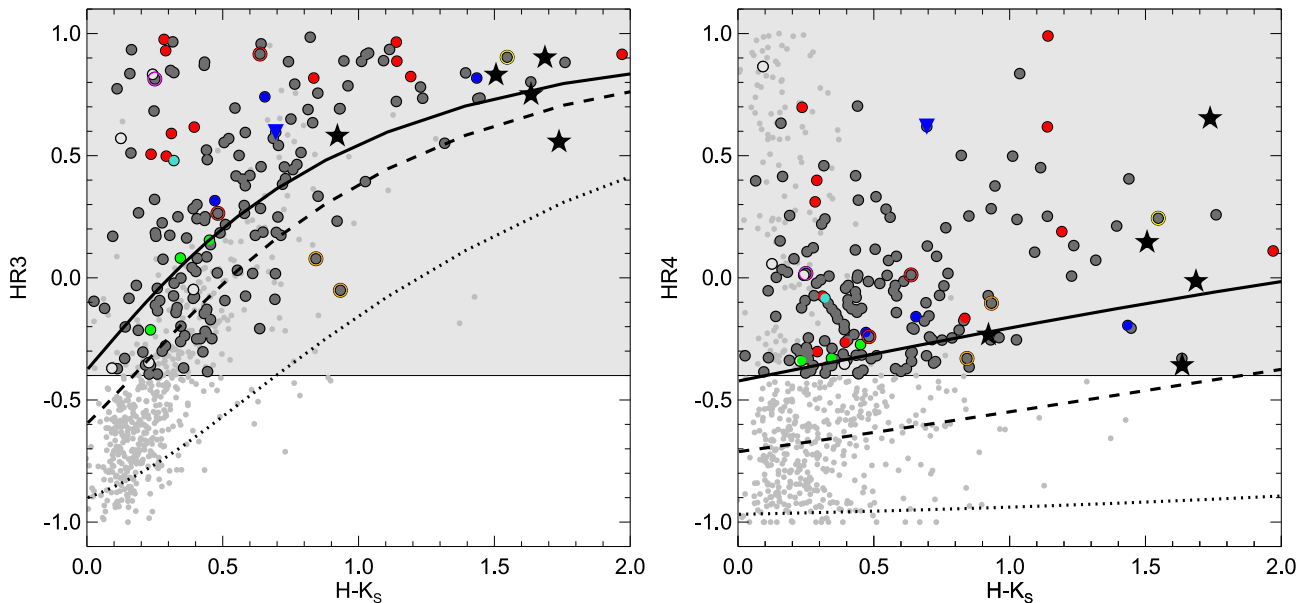


Figure 3. X-ray versus infrared colour–colour diagrams for soft (light grey) and hard sources (dark grey) compared to modelled values for active coronae (dotted), RS CVn binaries (dashed) and hard X-ray massive stars (solid). Note that we classified as hard sources those having both hardness ratios HR3 and HR4 greater than -0.4 . Plotted with filled circles are confirmed stars (2 B and 3 G stars) (light grey), HMXBs (red), Be stars (green), and WR stars (blue). The only AGN from the sample is shown as a filled blue upside down triangle and a Nova as a turquoise filled circle. Unidentified hard X-ray sources are shown in dark grey, surrounded by a coloured ring when a candidate classification of the source is available: candidate HMXBs (red), candidate YSO (yellow), candidate AGB stars (orange), candidate LMXB (magenta). Targets observed at the telescope are shown with a star symbol. See the text for more details.

are expected to have HR4 above -0.4 at any Galactic absorption (see right-hand panel in Fig. 3).

We selected sources with hard spectra, defined by HR3 and HR4, indicating thermal temperatures greater than 5 keV for N_{H} varying from 1×10^{20} to $3 \times 10^{22} \text{ cm}^{-2}$. The minimum temperature limit (HR limit) applied to exclude all normal stellar coronal emitters is the following:

$$\text{HR3} > -0.4 \ \& \ \text{HR4} > -0.4. \quad (2)$$

Selecting sources with HR3 and HR4 greater than -0.4 implies that sources are detected in hard X-rays due to either intrinsic hard X-ray emission (if $(H - K_s) \sim 0-0.1$) or a combination of intrinsic X-ray emission and high extinction (if $(H - K_s) > 0.1$). Sources with high values of HR3, HR4 and $(H - K_s)$ will probably have a high extinction.

A total of 173 X-ray sources fulfill the selection criteria (2) and we thus consider them hard X-ray sources. The remaining sources are considered soft X-ray sources in what follows. In Fig. 3, we show the location of soft and hard X-ray sources in the X-ray versus infrared colour–colour diagrams.

We investigated the nature of these 690 sources. We looked for possible entries in SIMBAD making use of XCatDB,⁶ and we complemented our search of known sources making use of Vizier. In Table 2, we list all the 690 associations. The content of the table is as follows. The *XMM-Newton* IAUNAME is followed by the X-ray positions, errors, count rates and HR. For each *XMM-Newton* source, the best 2MASS and GLIMPSE associations are given. 2MASS and GLIMPSE IAUNAMES, magnitudes, the distance between the X-ray and the infrared positions and the probability of identification are listed. The X-ray (2–12 keV) and the K_s fluxes

and the X-ray-to-infrared flux ratio are also given. The main SIMBAD name, the type of source and the spectral class are given when known. We finally give the spectral type reference used for the classification of each source. We present here an excerpt of the table which will be fully available in the electronic version.

We estimated the X-ray flux from the EPIC-pn count rate in the 2–12 keV band and using a count rate to energy conversion factor (ecf). Among others the ecf depends on the combination of camera and filter used, the X-ray emission mechanism, and the Galactic absorption (see Mateos et al. 2009). The ecf was computed assuming a thermal Bremsstrahlung model with $kT = 5 \text{ keV}$ and an absorption of $N_{\text{H}} = 10^{22} \text{ atoms cm}^{-2}$ ($\text{ecf} \sim 9.44 \times 10^{-12} \text{ count s}^{-1} (\text{erg cm}^{-2} \text{ s}^{-1})^{-1}$). The choice of the X-ray model and N_{H} value was done so as to be representative of hard X-ray emitting high-mass stars absorbed by the mean Galactic absorption of our sample, calculated from the mean $(H - K_s)$ and assuming sources have no intrinsic absorption and a colour $(H - K_s) = 0$ independent of their spectral type. A different N_{H} value and/or a different assumed model yields a different ecf, and thus X-ray fluxes presented in Table 2 are to be taken with caution.

As part of a pilot study, we were awarded with one night at the William Herschel Telescope (WHT, see Section 3). We selected targets visible for at least one hour ($\text{Dec.} > -30^\circ$, $15 \text{ h} < \text{RA} < 20 \text{ h}$). We prioritized infrared bright sources and went down the list until the end of the observations. We could acquire infrared spectroscopy for the following five sources: 3XMM J174347.4–292309, 3XMM J180920.3–201857, 3XMM J184541.1–025225, 3XMM J185210.0+001205 and 3XMM J190144.5+045914. From now on, we will refer to these sources as Source #1, Source #2, Source #3, Source #4 and Source #5, respectively). Finding charts used to identify the infrared target at the telescope are shown in Fig. 4. Observations and data reduction are described in the next section.

⁶ <http://xcatdb.unistra.fr/3xmm/>

Table 2. Infrared counterparts of X-ray sources.

Col.	Name	Contents					
1	3XMM	3XMM IAUNAME	J174347.4–292309	J180920.3–201857	J184541.1–025225	J185210.0+001205	J190144.5+045914
2	RA	SC_RA	265.94780	272.33492	281.42126	283.04190	285.43566
3	Dec.	SC_DEC	–29.38609	–20.31585	–2.87375	0.20143	4.98748
4	POSERR	SC_POSERR	1.21	0.35	0.44	0.81	0.58
5	CTS1	Count rate in 0.2–0.5 keV	0.00095	0.00037	0.00017	0.00093	0.00000
6	CTS2	Count rate in 0.5–1.0 keV	0.00000	0.00014	0.00025	0.00001	0.00014
7	CTS3	Count rate in 1.0–2.0 keV	0.00273	0.00065	0.00202	0.00138	0.00427
8	CTS4	Count rate in 2.0–4.5 keV	0.00288	0.00516	0.01109	0.00445	0.01528
9	CTS5	Count rate in 4.5–12.0 keV	0.01588	0.00583	0.03401	0.00247	0.01325
10	CTS8	Count rate in 0.2–12.0 keV	0.02245	0.01215	0.04753	0.00930	0.03295
11	CTS9	Count rate in 0.5–4.5 keV	0.00401	0.00536	0.01321	0.00599	0.01944
12	HR1	HR 1	–0.690	–0.572	–0.695	–0.833	1.000
13	HR2	HR 2	0.997	0.963	0.947	0.948	0.971
14	HR3	HR 3	0.557	0.831	0.902	0.751	0.581
15	HR4	HR 4	0.653	0.146	–0.014	–0.358	–0.233
16	HR1_ERR	Error in HR 1	0.545	0.215	0.283	0.265	1.346
17	HR2_ERR	Error in HR 2	0.158	0.058	0.085	0.096	0.047
18	HR3_ERR	Error in HR 3	0.163	0.033	0.021	0.062	0.042
19	HR4_ERR	Error in HR 4	0.099	0.038	0.034	0.085	0.044
20	2MASS	2MASS IAUNAME	17434750–2923098	18092038–2018572	18454111–0252257	18521006+0012073	19014457+0459147
21	d_2MASS	Distance to 2MASS assoc.	0.4	0.18	0.3	2.24	0.290
22	PROB_2MASS	Probability of 2MASS assoc.	0.989	0.998	0.994	0.670	0.998
23	J	2MASS J magnitude	11.145	11.923	11.562	11.333	11.148
24	H	2MASS H magnitude	7.897	9.225	8.700	9.487	9.763
25	K_s	2MASS K_s magnitude	6.159	7.719	7.014	7.852	8.841
26	eJ	2MASS J magnitude error	0.020	0.027	0.024	0.024	0.022
27	eH	2MASS H magnitude error	0.042	0.023	0.038	0.028	0.021
28	eK	2MASS K_s magnitude error	0.017	0.023	0.027	0.027	0.021
29	GLIMPSE	GLIMPSE IAUNAME	G359.4078+00.1051	G010.1568–00.3361	G029.7187–00.0316	G033.1949–00.0701	G038.5439–00.0120
30	d_GLIMPSE	Distance to GLIMPSE assoc.	0.320	0.34	0.12	2.35	0.110
31	PROB_GLIMPSE	Probability of GLIMPSE assoc.	0.998	0.999	0.999	0.966	0.995
32	I1	GLIMPSE 3.6 μm mag.	4.891	6.893		6.537	7.873
33	I2	GLIMPSE 4.5 μm mag.	4.798	6.227	5.346	5.462	7.589
34	I3	GLIMPSE 5.8 μm mag.	4.152	5.516	4.578	4.781	7.290
35	I4	GLIMPSE 8.0 μm mag.	4.137	5.322	4.284	4.469	6.981
36	eI1	GLIMPSE 3.6 μm mag. error	0.133	0.064		0.128	0.046
37	eI2	GLIMPSE 4.5 μm mag. error	0.046	0.086	0.067	0.066	0.043
38	eI3	GLIMPSE 5.8 μm mag. error	0.015	0.024	0.024	0.030	0.037
39	eI4	GLIMPSE 8.0 μm mag. error	0.019	0.024	0.027	0.021	0.025
40	f_x^a	X-ray flux in the 2–12 keV (ecf $\sim 9.44 \times 10^{-12}$)	$2.12\text{e}-13$	$1.15\text{e}-13$	$4.49\text{e}-13$	$8.78\text{e}-14$	$3.11\text{e}-13$
41	f_k	Infrared K_s flux	$3.18\text{e}-09$	$7.58\text{e}-10$	$1.45\text{e}-09$	$6.69\text{e}-10$	$2.69\text{e}-10$
42	$\log(f_x/f_k)$	X-ray to infrared flux ratio	–4.25	–3.86	–3.53	–4.01	–3.00
43	X-Type	S for soft or H for hard	H	H	H	H	H
44	NAME	Simbad name					
45	Class	Object class	Star(?)	WR*	WR*	Star(?)	Be*
46	SpT	Spectral type	M2I	WN7–8h	Ofpe/WN9	M2I	09e–B3e
47	References	Spectral type reference	This paper	This paper	This paper	This paper	This paper

Notes. The meaning of each line is given under the column *Contents*. ^aWe estimated the X-ray flux from the EPIC-pn count rate in the 2–12 keV band using a certain count rate to ecf. Among others the ecf depends on the combination of camera and filter used, the X-ray emission mechanism, and the Galactic absorption. The ecf was computed assuming a thermal Bremsstrahlung model with $kT = 5$ keV and an absorption of $N_{\text{H}} = 10^{22}$ atoms cm^{-2} (ecf $\sim 9.44 \times 10^{-12}$ count s^{-1} (erg cm^{-2} s^{-1})^{–1}). The choice of the X-ray model and N_{H} value was done so as to be representative of hard X-ray emitting high-mass stars absorbed by the mean Galactic absorption of the sample, calculated from the mean $(H - K_s)$ and assuming sources have no intrinsic absorption and a colour $(H - K_s) = 0$ independent of their spectral type. A different N_{H} value yields a different ecf, X-ray fluxes are thus to be taken with caution. Class and spectral type come from the literature with exception of the five sources studied in this paper. When available the main Simbad name is given. We present here an excerpt of the table which will be fully available in the electronic version.

3 INFRARED SPECTROSCOPY

WHT/LIRIS. Infrared spectroscopic observations were carried out at the WHT equipped with the near-IR imager/spectrograph Long-slit Intermediate Resolution Infrared Spectrograph (LIRIS) on the 2012 May 3 (UT) for five of our sources. We obtained spectra with gratings *J*, *H* and *K* with a slit width of 0.75 arcsec (see Table 3). We positioned our targets at two nodding points around which we applied small offsets in order to subtract the sky and telescope/mirror emissions. The total exposure times were adjusted to obtain a signal

to noise of about 100. We used standard MIDAS procedures to flat-field correct and extract our spectra, using the optimal extraction method described by Horne (1986). We took Xenon-Argon arc lamp exposures to calibrate in wavelength, and obtained spectra of the standard stars HIP89218 and HIP93118 at the beginning, middle and end of the observations to clean our spectra from telluric lines. Flux calibration was not possible due to a technical problem of the CCD. Spectra are shown in Fig. 5.

We identified spectral lines in the infrared spectra using a diversity of references (Morris et al. 1996; Figer, McLean & Najarro

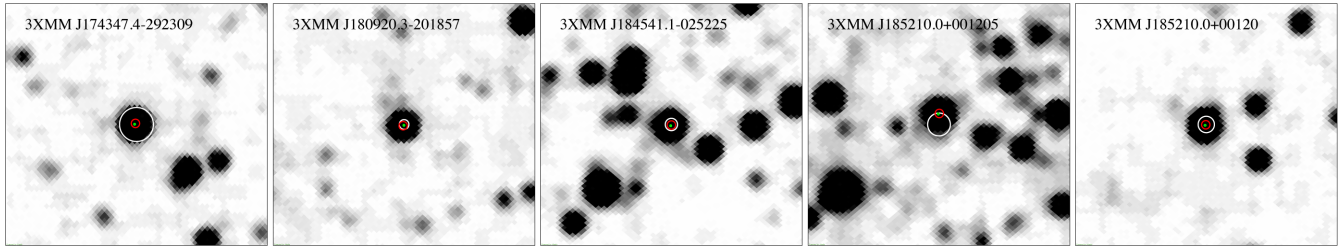


Figure 4. 2 arcmin square 2MASS *J*-band image centred around the five observed targets at the WHT. Positions and 3σ errors are shown with circles, in white for 3XMM, in green for 2MASS and in red for GLIMPSE detections. Following the standard convention, north is up and east is left.

Table 3. Observational technical details.

Tel.	Inst.	Grism	Slit (arcsec)	Spectral range (Å)	Spectral res. (Å)	Date (dd/mm/yyyy)
WHT	LIRIS	<i>J</i>	0.75	11 690–13 530	3.6	03/05/2012
WHT	LIRIS	<i>H</i>	0.75	15 160–17 790	5.2	03/05/2012
WHT	LIRIS	<i>K</i>	0.75	20 490–24 110	7.2	03/05/2012

1997; Hanson, Rieke & Luhman 1998; Clark & Steele 2000; Förster Schreiber 2000; Steele & Clark 2001) and with help of the atomic data bases NIST⁷ and <http://www.pa.uky.edu/peter/atomic/>.

4 MAGPIS MID-IR AND RADIO IMAGES

We looked for possible mid-IR and radio emission of our sources in the Multi-Array Galactic Plane Imaging Survey (MAGPIS; Helfand et al. 2006) which imaged portions of the first quadrant of the Galaxy at 20 and 90 cm with the Very Large Array (VLA). We retrieved images from the MAGPIS web site,⁸ which also includes 6 cm VLA, 21 μm Midcourse Space Experiment (MSX; Egan et al. 2003), and 24 μm *Spitzer* MIPS GAL (Carey et al. 2009) images. In this way, we created composite colour-coded images of 10 arcmin around the five targets studied in this paper (see Figs 6–10).

5 SOURCE CLASSIFICATION

In this section, we describe the spectral type and stellar parameters for each of the sources observed at the WHT. We estimated the X-ray flux in the 0.2–12 keV band assuming a thermal model with $kT = 5$ keV (see Section 2.3) and the Galactic N_{H} we obtained for each object. All parameters are given in Table 4 and some important lines with their equivalent width (EW) are listed in Table 5.

5.1 3XMM J174347.4–292309 (Source #1)

The infrared spectra of Source #1 reveal absorption of many atomic lines typical of late K and early M stars, such as Si I, Mg I, Fe I, K I, Al I, Na I, Ca I and the CO band (see Fig. 5). We used the EW of the CO band-head at 16 187 Å and the Fe absorption lines at 22 263 and 22 387 Å as indicators of the temperature and luminosity class of the star. We compared the depth of the CO band head ($\text{EW}_{\text{CO } 16187\text{Å}} = 6 \pm 1$ Å) and the sum of the EWs of the Fe I 22 263 Å and the Fe I at 22 387 Å lines ($\text{EW}_{\text{Fe } 22263\text{Å}} + \text{EW}_{\text{Fe } 22387\text{Å}} = 4 \pm 1$ Å) with values observed in dwarf, giant and supergiant stars (Förster

Schreiber 2000). These values are consistent with a red giant or a red supergiant (RSG) with effective temperature close to 3500 K, corresponding to a spectral type M2 III–I. The EW of the CO-bandhead at 2.3 μm ($\text{EW}_{\text{CO } 2.3\mu\text{m}} = 41 \pm 5$ Å) is compatible with a supergiant star (Negueruela et al. 2010) although such high values have also been found in some giant stars (Messineo et al. 2014).

In order to construct the spectral energy distribution (SED), we complemented the 2MASS and GLIMPSE photometric values with information gathered from VizieR. At a distance of 1.6 arcsec from Source #1 there is a *WISE* detection (Wright et al. 2010), WISE J174347.51–292309.5 (Cutri 2012). *WISE* provides photometry for the whole sky in four bandpasses centred at 3.4, 4.6, 12 and 22 μm (*W1*, *W2*, *W3*, and *W4*, respectively). With magnitudes equal to 5.458 ± 0.038 , 4.118 ± 0.042 , 3.982 ± 0.038 , 2.927 ± 0.075 in filters *W1*, *W2*, *W3*, and *W4*, respectively, WISE J174347.51–292309.5 *W1* and *W2* magnitudes are not consistent with GLIMPSE I1 and I2 magnitudes. This discrepancy is likely due to the higher spatial resolution of the GLIMPSE survey compared to *WISE*, rather than due to photometric variability. Nearby resolved GLIMPSE sources may indeed be blended and contribute to *WISE* magnitudes. We fitted the SED of Source #1 with two models of spectral types M0 III and M2 I from Castelli & Kurucz (2004), with $(T_{\text{eff}}, \log(g)) = (3800 \text{ K}, 1.34)$ and $(T_{\text{eff}}, \log(g)) = (3450 \text{ K}, -0.06)$, respectively. The $(H - K_s)$ colour indicates a large extinction, $22 < A_V < 27$. We fixed extinction to $A_V = 26$ magnitudes, equal to the total interstellar extinction in the area (Schultheis et al. 1999). According to the empirical spectral type radius relation from van Belle et al. (1999), assuming a giant star, the radius is $40_{-7}^{+9} R_{\odot}$, for an error in the spectral type determination of ± 1 subtype. From the fitting flux scaling factor, we estimated a distance to the star of 310_{-50}^{+70} pc. We are not aware of the existence of such a nearby high-extinction region and we thus conclude that the star must be a supergiant. Supergiant stars exhibit a wide range of luminosities (see e.g. Meynet & Maeder 2000; Marigo et al. 2008) and as a result a wide range of absolute magnitudes is expected and observed (Levesque et al. 2005). Therefore, no reliable distance may be derived from the photometry. The high extinction observed indicates that the source must be rather distant. According to Marshall et al. (2006) the A_K extinction in the

⁷ <http://www.nist.gov/pml/data/asd.cfm>

⁸ <http://third.uclnl.org/gps/>

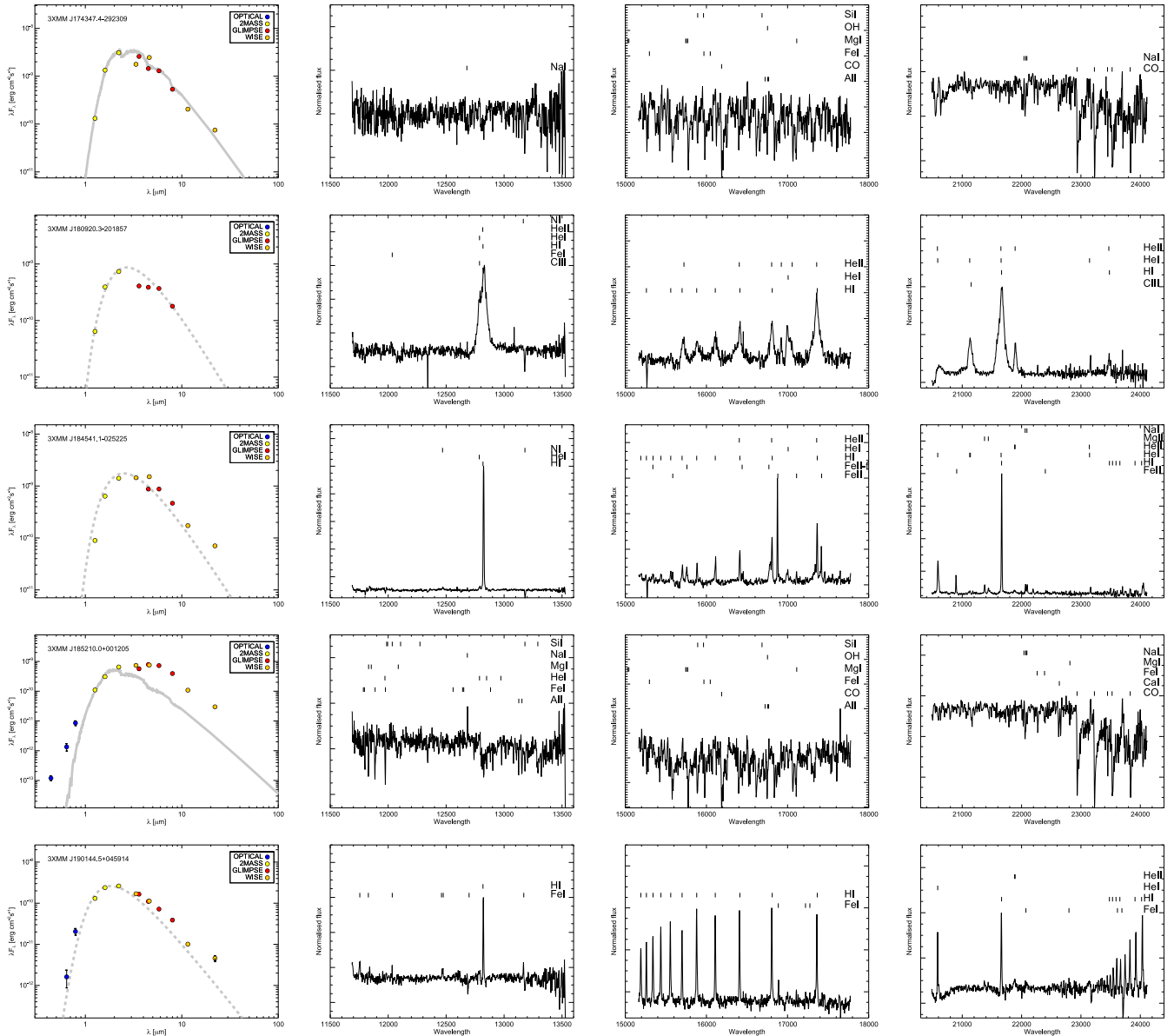


Figure 5. Observed SED (coloured dots) compared to the best-fitting absorbed model or Rayleigh Jeans distribution (solid or dashed grey line), followed by the WHT infrared spectra in the J , H and K bands. From top to bottom: Source #1, Source #2, Source #3, Source #4, and Source #5.

line of sight (l, b) = ($359^{\circ}.5, 0^{\circ}$) reaches a value close to 2.5 at a distance larger than 4.5 kpc. At a distance of 4.5 kpc, the source absolute magnitude M_K is equal to -10.07 , a value consistent with those of RSG stars (Levesque et al. 2005). Fixing the distance, from the best SED fit, we obtained a radius of about $640 R_{\odot}$, a value consistent with known RSG stars. A larger distance to the source would imply a brighter absolute magnitude and a larger radius.

Source #1 was detected in two different observations with a mean count rate of 0.022 ± 0.006 cts s^{-1} in the 0.2–12 keV band. We derived an unabsorbed X-ray luminosity of $L_X > 6 \times 10^{32}$ erg s^{-1} ($N_H = 4.6 \times 10^{22}$ cm $^{-2}$). No intrinsic absorption was assumed.

On five occasions, *Chandra* detected the hard source CXOGC 174347.4–292309 (RA = 17:43:47.50, Dec. = $-29^{\circ}:23^{\circ}:09.9$, r_{95} per cent = 0.7 arcsec) (Hong et al. 2009; Mauerhan et al. 2009; Munro et al. 2009) at a distance of 1.7 arcsec from the *XMM-Newton*

position. Given the positional errors of Source #1 (1.2 arcsec) and of CXOGC 174347.4–292309, the *Chandra* and *XMM* detections are likely to be associated with the same source. Importantly, the improved *Chandra* position is consistent with the GLIMPSE candidate (Munro et al. 2009). Long-term X-ray flux variations were detected between different *Chandra* observations (Munro et al. 2009). The ratio between maximum and minimum observed fluxes is in the range 2.3–8.2, and has an associated time span of approximately 5 yr. Maximum flux was detected in 2006 September. The two *XMM-Newton* observations in which the source was detected span less than 1 yr, both of them in 2006 (February and September). No significant flux variation was detected between these two observations nor within the observations. Assuming the X-ray luminosity of $L_X = 6 \times 10^{32}$ erg s^{-1} (derived from the *XMM-Newton* observations) as a maximum value the ratio between the minimum to maximum flux observed by *Chandra* implies a minimum X-ray luminosity of $L_X \sim 7.3 \times 10^{31}$ erg s^{-1} .

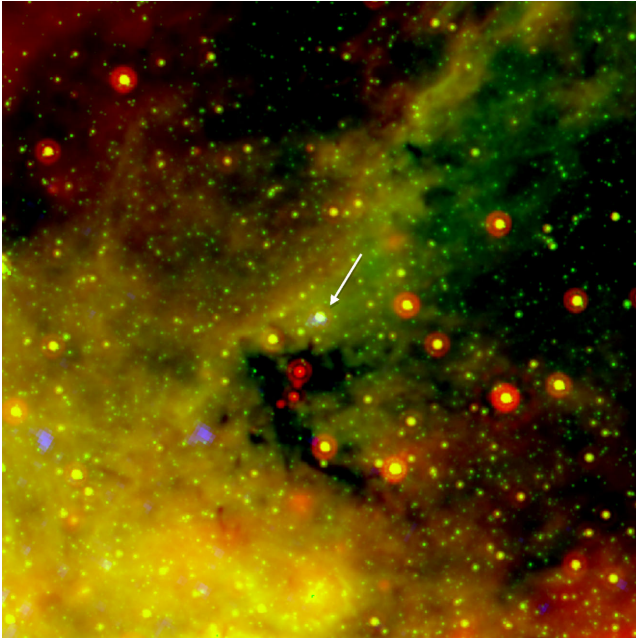


Figure 6. 10 arcmin square RGB image centred around Source #1 (red = 24 μm , green = 8 μm GLIMPSE, blue = EPIC-pn *XMM-Newton*). North is up and east is left.

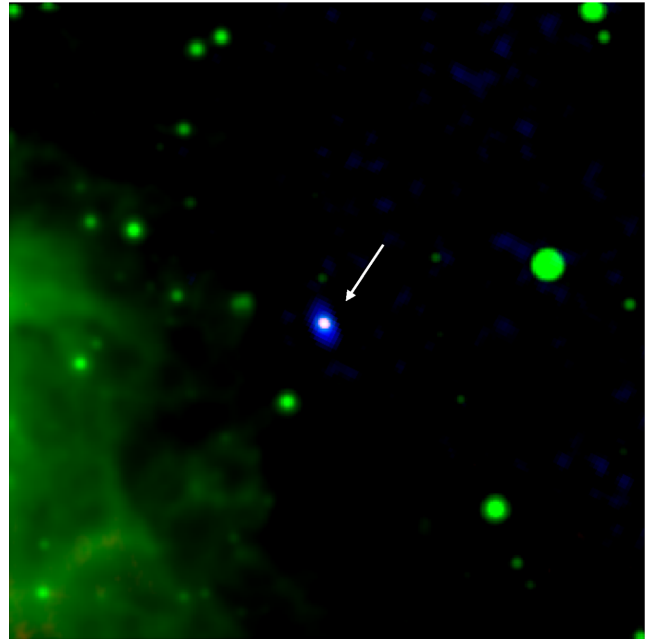


Figure 8. 10 arcmin square RGB image centred around Source #3 (red = radio 20 cm, green = 24 μm , blue = EPIC-pn *XMM-Newton*). North is up and east is left.

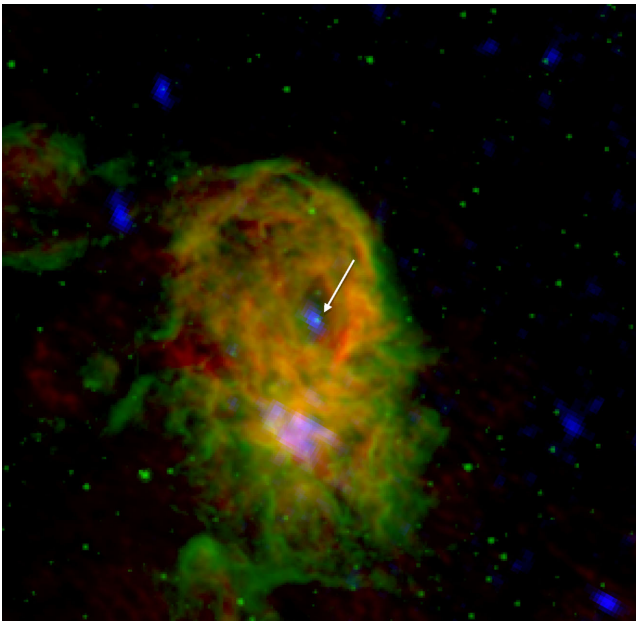


Figure 7. 10 arcmin square RGB image centred around Source #2 (red = radio 20-cm, green = I3-GLIMPSE filter, blue = EPIC-pn *XMM-Newton*). North is up and east is left.

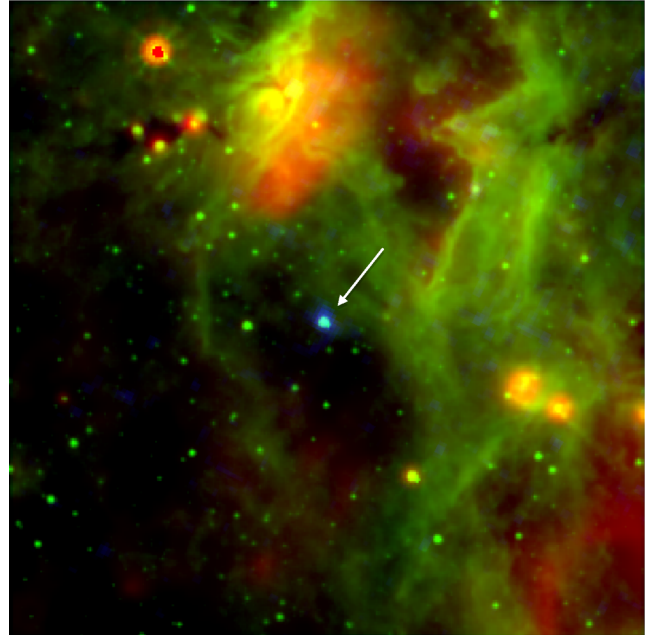


Figure 9. 10 arcmin square RGB image centred around Source #4 (red = MIPS GAL 24 μm , green = GLIMPSE 8.0 μm , blue = EPIC-pn *XMM-Newton*). North is up and east is left.

5.2 3XMM J180920.3–201857 (Source #2)

The WHT J -, H - and K -band spectra of Source #2 reveal very broad emission lines, in particular from the complex at 12 788–12 818 \AA , formed by C III, He I, He II, and H I (see Fig. 5), and from the complex at 21 652–21 663 \AA , formed by He II, He I and H I. The presence of such emission lines is typical of WN stars (Shara et al. 2009). The strong emission He II λ 21 891 \AA line indicates a WN7–8h spectral type. We estimated the ratio of the EW of the 21 891 \AA He II line to the EW of the complex at 21 663 \AA to be 0.1, and between the

21 891 \AA and the 21 126 \AA He II lines to be 0.5. These values are in agreement with a WN8 spectral type (Figer et al. 1997; Rosslowe & Crowther 2015).

We followed the method in Crowther et al. (2006) to determine the distance to the source. From the 2MASS colours and assuming intrinsic colours of WN7–8h stars from Crowther et al. (2006), we calculated the colour excess $E(J - K_s)$ and $E(H - K_s)$. We used the extinction relations $A_K = 0.67^{+0.07}_{-0.06} \times E(J - K_s)$ and $A_K = 1.82^{+0.30}_{-0.23} \times E(H - K_s)$ from Indebetouw et al. (2005) to

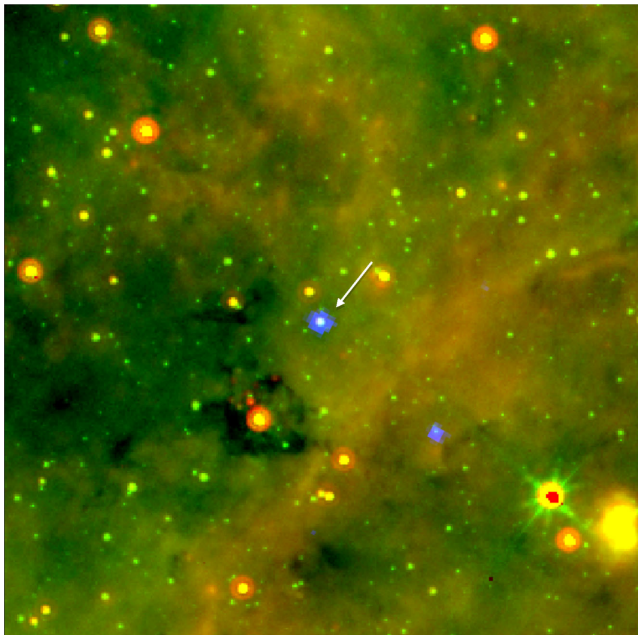


Figure 10. 10 arcmin square RGB image centred around Source #5 (red = MIPS GAL 24 μm , green = GLIMPSE 8.0 μm , blue = EPIC-pn *XMM-Newton*). North is up and east is left.

derive a mean value $A_K = 2.63^{+0.35}_{-0.28}$. Using the extinction relation $A_K = 0.114 \times A_V$ for $R_V = 3.1$ from Cardelli, Clayton & Mathis (1989), we estimated $A_V = 23 \pm 3$. Rosslowe & Crowther (2015) revised the infrared absolute magnitudes of the largest sample of WR stars to date. For WN7ha and WN9ha stars they obtained a mean value of M_K of -7.24 and -6.34 , respectively, with a spread of about 0.3 mag at each subtype. From the observed K_s magnitude, the mean A_K and assuming an absolute magnitude M_K equal to the mean value for WN7a and WN9ha stars ($M_K = -6.79 \pm 0.42$), we estimated a distance to the source of $2.4^{+0.8}_{-0.7}$ kpc.

We compared the observed infrared spectra with model spectra from Hamann & Gräfener (2004) and found a best match for a WNL with an effective temperature of about 40 000 K. Using this T_{eff} and a distance to 2.4 kpc implies a radius of $30 \pm 10 R_{\odot}$. Fixing the extinction and distance, no blackbody can fit the observed SED, even when discarding the GLIMPSE I1 and I2 magnitudes which could be confused with surrounding nebular emission. We therefore left the extinction as a free parameter and obtained a best fit for $A_K \sim 3.5$ ($A_V \sim 30$). Assuming a mean absolute magnitude for WN7a and WN9ha, we obtained a distance ≈ 1.6 kpc, which is an extremely small distance for such a high extinction.

In Fig. 7, we show a 10 arcmin composite colour image around Source #2. The observed infrared nebulosity is likely associated with Source #2, i.e. the strong wind and ionizing photons produced by this hot massive star blow away the surrounding material forming a cavity around the star, and ionizing the gas in the nebulae, which is also seen as radio emission (see Fig. 7). Indeed, the X-ray source is in the infrared dark cloud SDC G10.156–0.340 (IRDC; Peretto & Fuller 2009), embedded in an infrared bubble (N 1 from Churchwell et al. 2006; Deharveng et al. 2010). According to Deharveng et al. (2012), this bubble is in an H II region that forms part of a more complex structure, the star-forming region W 31 at spectrophotometric distance 3.4 ± 0.3 kpc (Blum, Damiani & Conti 2001). At a distance of about 1.5 arcmin from Source #2 the source 3XMM J180926.9–201930 was detected by the *XMM-Newton*

as an extended X-ray source. This extended source has a very hard spectrum and is likely associated with the OB cluster W31 IR Cluster. Stead & Hoare (2011) estimated the cluster to be formed by about 35 candidates with extinction $A_j = 4.3^{+1.4}_{-0.6}$ ($A_K = 1.7^{0.6}_{-0.2}$). Although the lower limit of the extinction A_K we obtained for Source #2 is consistent with the upper limit of such a value, the distance to the cluster is higher than to Source #2 by at least 500 pc. Moreover, in a recent study Sanna et al. (2014) find a distance to the cluster of 5.0 ± 0.5 kpc based on parallax measurements, a value inconsistent with our distance estimate for Source #2. It is a bit surprising that Source #2 has a higher extinction than W31 while being foreground to W31. Assuming that the source is associated with the cluster, i.e. located at 5 kpc and is absorbed by $A_K \sim 1.7$ implies $M_K \sim -8.39$. Under these conditions, no blackbody can fit the observed SED. Leaving the extinction as a free parameter yields $A_K \sim 3.5$ and $M_K \sim -9.29$, a value higher than observed in typical WRs.

Source #2 was detected in 13 different observations with a mean count rate of 0.012 ± 0.006 cts s^{-1} and with no significant flux variation. Assuming $A_K = 2.63^{+0.35}_{-0.28}$, corresponding to $N_H \sim 5.5 \times 10^{22}$ cm^{-2} (Predehl & Schmitt 1995), the unabsorbed X-ray luminosity is in the range $4 \times 10^{31} - 4 \times 10^{32}$ erg s^{-1} depending on the assumed distance (1.6–5 kpc) to the source. The bolometric luminosity $\log(L_{\text{bol}}/L_{\odot})$ is in the range of 6.29–7.29 ($\text{BC}_K = -4.2$, Mauerhan et al. 2010) yielding $\log(L_X/L_{\text{bol}}) = -8.2$, a value lower than the mean value for WN stars but within the observed range (Mauerhan et al. 2010).

5.3 3XMM J184541.1–025225 (Source #3)

The infrared spectra of Source #3 reveal strong and narrow emission lines of H I, blended with He I, and of some ionized species, in particular Fe II and Mg II. The *H*-band spectra displayed the forbidden line [Fe II] at 16 770 Å blended with the H I (11–4) line. The absence of the 16 923 Å He II line implies a spectral type later than O. The spectra also shows Na I 22 060 and 22 090 Å in emission. These lines are typical of Ofpe/WN9 and early Be and B[e] stars (Morris et al. 1996; Hanson et al. 1998). Whether the source is a luminous blue variable (LBV), i.e. a source displaying spectroscopic variations between both spectral types, is an open question, and more observations are required to elucidate the nature of the source.

The 90 percent error circle of Source #3 also contains WISE J184541.11–025225.5 which is probably associated with the GLIMPSE identification. In Fig. 5, we present the observed SED. We determined the mean extinction following the same procedure as for Source #2. The mean A_K value is $3.0^{+0.4}_{-0.3}$. We assumed an effective temperature of 20 000 K and a radius of 79 R_{\odot} , corresponding to the Ofpe/WN9 star CXOGC J174516.1–284909 (Mauerhan et al. 2010) and fitted a blackbody curve. From the best fit, we obtained a distance to the source of 2.4 ± 0.3 kpc, implying an absolute magnitude $M_K = -7.9 \pm 0.1$. Negueruela et al. (2011) studied in detail several nearby sight-lines. These areas showed moderate extinction up to distances of 3–3.5 kpc and with an abrupt increase between 6 and 7 kpc ($A_K > 1.5$) due to dark clouds associated with the Scutum arm. At the calculated A_K , the source would be even more distant. Assuming the source is at about 2.4 kpc it would be in the interarm region. Nevertheless, it could be that the source has some local obscuration and/or emission, especially since the source has $[W1]-[W4] = 2.6$, a colour atypical of interstellar absorption.

About 3.6 arcsec from Source #3 there is the radio emitter GPS5 029.718–0.031, detected in the 5 GHz VLA survey of

Table 4. Parameters.

Name 3XMM J	SpT	T_{eff} (K)	Rad (R_{\odot})	A_V	N_H ($\times 10^{22} \text{ cm}^{-2}$)	H	K_s	M_K	d (kpc)	Count rate (cts s^{-1})	$L_X(0.2\text{--}12 \text{ keV})$ ($10^{32} \text{ erg s}^{-1}$)	Nature
174347.4–292309	M2 I	3500	640	~ 26	4.6	7.897	6.159	-10.2^b	> 4.5	0.022 ± 0.006	> 6	?
180920.3–201857	WN8	40 000	30 ± 10	23 ± 3	4.1 ± 0.5	9.225	7.719	-6.79^a to -9.29	1.6–5	0.012 ± 0.006	0.4–4	WCB
184541.1–025225	Ofpe/WN9	20 000	79	26 ± 3	4.6 ± 0.5	8.700	7.014	-7.9 ± 0.1	2.4 ± 0.3	0.047 ± 0.007	2.3–5.3	WCB/SFXT
185210.0+001205	M2 I	3500	430	~ 15	5.4 ± 0.2	9.487	7.852	-9.06	11	0.009 ± 0.002	< 15	?
190144.5+045914	Be	–	–	15 ± 2	2.7 ± 0.2	9.763	8.841	-3.15 to -4.43	1.0–1.9	0.033 ± 0.002	0.9–3.0	γ -Cas

Notes. We list the 3XMM IAU/NAME of the five targets observed at the telescope, the spectral type of the infrared association derived from the spectra taken at the WHT, effective temperature and radius derived from the SED fit, A_V estimated from the infrared colour (see the text for more details), N_H calculated using the relation from Predehl & Schmitt (1995). Observed H and K_s 2MASS magnitudes are followed by the absolute magnitude in the K_s band. We adopted absolute magnitudes from Crowther et al. (2006)^a and Covey et al. (2007)^b. Distances are calculated from the adopted absolute magnitudes. Finally, we list the count rate and X-ray luminosity in the 0.2–12 keV band, followed by the likely nature of the X-ray source.

the galactic plane (Becker et al. 1994). The radio position and flux of GPS5 029.718–0.031 is consistent with those of the compact radio source [WBH2005] 29.719–0.031 (White, Becker & Helfand 2005), about 1 arcsec away from the X-ray position but within the combined position errors. The GLIMPSE source is probably associated with the radio source GPS5 029.718–0.031 (Hoare et al. 2012). The radio emission might be ascribed to a massive young stellar object (MYSO) associated with collimated jets and winds, or it could originate in a new born H II region. The detected radio emission at 6 and 21 cm (Becker et al. 1994) is consistent with a flat spectral index $\alpha \sim 0$ ($S_\nu \propto \nu^\alpha$), indicating a non-thermal emission, and excluding a possible MYSO nature of the source, objects with a typical α value $\sim +0.6$. X-ray emission associated with high-mass stars has been suggested as an ionizing source of UCH II regions (Hofner et al. 2002). We conclude that the radio emission detected in the combined X-ray plus radio 90 per cent confidence error circle of Source #3 is associated with a radio-loud ultracompact H II region (UCH II). This UCH II region, detected at radio wavelengths could explain the observed [W1]–[W4] colours. We adopted a distance to the source of 2.4 kpc.

The three X-ray detections of Source #3 have a mean count rate equal to 0.047 ± 0.007 cts s^{-1} in the 0.2–12 keV band, implying an unabsorbed X-ray luminosity $L_X = 3.7_{-1.4}^{+1.6} \times 10^{32} \text{ erg s}^{-1}$. We assumed the bolometric correction from Mauerhan et al. (2010) derived for the Ofpe/WN9 star CXOGC J174516.1–284909 and obtained $\log L_{\text{bol}} = 6.21 L_{\odot}$, and thus $\log(L_X/L_{\text{bol}}) = -7.2$, value consistent with the canonical value of -7 .

5.4 3XMM J185210.0+001205 (Source #4)

As for Source #1, the infrared spectra of Source #4 reveal absorption lines of many atomic species typical of late K and early M stars (Si I, Mg I, Fe I, K I, Al I, Na I, Ca I and the CO band, see Fig. 5). Besides the Na I 12 683 Å emission line in the *J*-band spectrum, no other emission line could be identified in the spectra. Following the same approach as for Source #1, we measured the EW of several absorption lines to determine the spectral type and luminosity class of the star. With an $\text{EW}_{\text{CO}23227\text{Å}} = 20 \pm 1$ Å, an Fe I 22 263 Å to Fe I at 22 387 Å EW ratio equal to 5 ± 2 and $\text{EW}_{\text{CO}2.3\mu\text{m}} = 43 \pm 5$ Å the spectrum of the star is consistent with that of an RSG with effective temperature close to 3500 K, corresponding to a spectral type M2 I (Förster Schreiber 2000; Negueruela et al. 2010).

Source #4 has the optical counterpart USNO 0902-0385469 in the USNO–B1.0 catalogue (Monet et al. 2003), at a distance of 0.26 arcsec and mean magnitudes equal to 20.9, 17.7, and 15.2 in the *B*, *R* and *I* filters, respectively. The source was detected in the 2XMMi-DR3 and was already listed as having IR and optical counterparts by Nebot Gómez-Morán et al. (2013). At a distance of about 2 arcsec from Source #4 there is the *WISE* detection WISE J185210.06+001207.3 with magnitudes 6.411 ± 0.038 , 5.404 ± 0.025 , 4.675 ± 0.017 , and 3.923 ± 0.040 in filters W1, W2, W3 and W4, respectively. *WISE* magnitudes are in agreement with GLIMPSE magnitudes. We constructed the SED and concluded that it cannot be explained by a single atmosphere component when comparing with the Castelli & Kurucz (2004) model with $T_{\text{eff}} = 3450$ K and $\log(g) = -0.06$, corresponding to a spectral type M2 I. Assuming an intrinsic colour ($J - K_s$) of 0.87 equal to the values found for M2 I stars (Negueruela et al. 2010), we derived an extinction $A_K \sim 1.75$ ($A_V \sim 15$). According to Marshall et al. (2006), the extinction in the line of sight (*l*, *b*) = (33°25', 0°) reaches that value at about 11 kpc, giving us an upper limit on the distance to the

Table 5. EWs (in Å) of some important emission lines (in μm).

Name 3XMM J	He II+Pβ	He II	He I	He I	He I/NI II	He II+Brγ	He II
	1.281	1.692	1.700	2.058	2.115	2.165	2.189
180920.3–201857	71	2	9	–	19	64	8
184541.1–025225	90	–	3	17	–	40	2
190144.5+045914	6	–	1	9	–	10	3

source. No single atmosphere model is able to reproduce the observed SED from the *B* to the *W4* bands. To match the blue part of the SED (*B* to *K_s* bands) the needed attenuation is $A_V \sim 18$, displaying an excess at longer wavelengths. To match the infrared part of the SED (*H* to *W4* bands) requires $A_V \sim 28$ displaying an excess at shorter wavelengths. The extinction inferred from the infrared colours is closer to the extinction obtained through SED fitting in the blue part of the spectra than to the red part. Source #4 is in a dark cloud (Peretto & Fuller 2009) within a molecular cloud and an H II region (Anderson et al. 2009), which is consistent with a high extinction. It could be that the GLIMPSE source is confused with this H II region at longer wavelengths, explaining the disagreement between the observed SED and that of an RSG star. Assuming an upper limit of 11 kpc to the source and an extinction of $A_K \sim 1.75$, we obtained an absolute magnitude of $M_J = -8.2$. From the SED best fit to the blue part of the spectra, we estimated that the radius of the source is around $430 R_\odot$.

Source #4 was detected in two *XMM–Newton* observations, with mean count rate 0.009 ± 0.002 cts s^{-1} , implying an X-ray luminosity of 1.5×10^{33} erg s^{-1} at a distance of 11 kpc. No variability was observed between the two observations.

5.5 3XMM J190144.5+045914 (Source #5)

The infrared spectra of Source #5 show the H I Brackett and Pfund series in emission, which together with the He I also seen in emission, indicate that the source is probably an early-type Be star, with spectral type O9e–B3e (Clark & Steele 2000; Steele & Clark 2001), where the X-ray and UV photons originating from the hot B star ionize the circumstellar disc giving rise to strong hydrogen recombination emission lines. Photospheric absorption lines are visible in the *K*-band spectrum. Emission lines of He II, and Fe I are also present in the spectra (see Fig. 5).

The GLIMPSE and MIPS GAL images at 8 and 24 μm, respectively, revealed an extended dark cloud in the direction of Source #5 (see RGB composite image in Fig. 10). At 8 μm, emission is dominated by poly-cyclic aromatic hydrocarbons, and at 24 μm emission is dominated by very small dust grains. The emission from this warm dust can explain the high extinction observed for Source #5, for which we derived $A_K = 1.69^{+0.21}_{-0.15}$ ($A_V = 15 \pm 2$) magnitudes from the (*H*–*K_s*) colour and assuming the intrinsic colours of O9.5 stars from (Martins & Plez 2006, note that these colours are independent of the stellar luminosity class). However, the source was also detected in the AllWISE catalogue, AllWISE J190144.57+045914.8, with magnitudes that are not consistent with a reddened Rayleigh distribution (see Fig. 5), suggesting some local excess, probably from the circumstellar Be disc. Therefore, we cannot use the observed infrared colour as a reliable indicator of the extinction and the A_V value should be considered as an upper limit to the extinction. At shorter wavelengths, the USNO photographic magnitudes are not accurate enough to constrain the reddening.

Late-O and early-B supergiants show absorption lines in the infrared spectra, while the brightest blue supergiants show spectra

with strong wind emission lines (Hanson et al. 2005), both inconsistent with our infrared spectra. Since we do not know the luminosity class of the star, we assumed different tabulated magnitudes for O9.5 stars with luminosity classes V and III from Martins & Plez (2006) and derived maximum distances of about 1.0–1.9 kpc depending on the luminosity class. The possible link of this system to the class of γ -Cas analogues will be discussed in Section 6.1

X-ray emission from Source #5 was first detected by ASCA, AX J190144+0459 (Sugizaki et al. 2001), as extended diffuse emission, however, the extension was not confirmed by subsequent *XMM–Newton* observation (Yamaguchi et al. 2004). Assuming a power-law model with $\Gamma = 1.7$, Yamaguchi et al. (2004) derived $N_H = 3.3 \times 10^{22}$ cm^{-2} and an N_H corrected flux of 5.1×10^{-13} erg cm^{-2} s^{-1} in the 0.5–10 keV band. In the range of distances, we derived this implies $L_X \sim 6.4 \times 10^{31} - 2.1 \times 10^{32}$ erg s^{-1} . Corral et al. (2015) fitted the source to different models and present the results in the *XMM–Newton* spectral-fit catalogue.⁹ In the energy range from 0.5 to 10 keV, the best fit is found for an absorbed thermal plasma with $kT = 9.27^{+3.69}_{-2.23}$ keV, $N_H = 2.99^{+0.59}_{-0.28} \times 10^{22}$ atoms cm^{-2} , with a corresponding absorption corrected flux of $3.14 \pm 0.34 \times 10^{-13}$ erg cm^{-2} s^{-1} , implying L_X in the range of $\sim 4.0 \times 10^{31} - 1.3 \times 10^{32}$ erg s^{-1} .

6 DISCUSSION

In this section, we discuss the possible origin of the hard X-ray emission observed in these five X-ray sources, where infrared counterparts pointed to three high-mass stars and two descendants of high-mass stars. We then discuss the nature of all the hard X-ray sources found in this study.

6.1 High-mass stars

The origin of hard X-ray emission in massive stars is still in debate. There are mainly three competing scenarios: intrinsic X-ray emission, accretion on a compact object and colliding winds in a binary system. These three scenarios have been discussed in great detail in Mauerhan et al. (2010). We here briefly summarize the main properties of systems in the different scenarios.

The intrinsic X-ray emission of early-type stars is typically thermal, soft ($kT \sim 0.5$ keV) and due to radiative shocks occurring within the high-velocity wind (Lucy & White 1980). This mechanism is thought to be at work in a wide range of massive stars, including WR stars (Skinner et al. 2010). Unusually hard X-ray emission, although rare in single objects, has been detected in some massive stars (e.g. θ^1 -Orionis C). As a possible explanation to the hard X-ray emission ($kT \sim 3$ keV), it has been suggested that the high magnetic fields observed (≥ 1 kG) could confine and channel the stellar wind from the poles into the equator where a shock

⁹ <http://xraygroup.astro.noa.gr/Webpage-prodec/index.html>

could heat the plasma up to 10^7 K, thus producing hard X-ray emission (Gagné et al. 2005). Mauerhan et al. (2010) calculated that the strength of the magnetic field should be $\gtrsim 5$ kG in order to confine the fast winds observed in the WR and O stars of their sample, which is similar to ours. Since so far there is no observational evidence of such high magnetic fields in WR stars, we disregard this scenario for our WR candidates.

In the second scenario, a compact object accretes matter from a massive star, i.e. HMXBs. There are three types of HMXBs: those accreting material from the circumstellar Decretion disk of a Be star (Be-HMXB), those accreting material from the wind of a supergiant high mass X-ray binaries (SGXBs), and those accreting from a Roche lobe filling supergiant star (Chaty 2011). Since Be-HMXBs display $L_X > 10^{33}$ erg s $^{-1}$, the low observed X-ray luminosity of the Be star counterpart of Source #5 indicates that the source is most probably not a classical Be-HMXB in quiescence.

Supergiant high-mass X-ray binaries, i.e. a neutron star or a black hole accreting from the strong radiative wind emitted by an OB supergiant star or by a WR star, have persistent X-ray luminosities $L_X \sim 10^{35}$ – 10^{36} erg s $^{-1}$, show rapid variations and are rather constant on long time-scales (see Sguera et al. 2006, and references therein). The X-ray luminosities observed in our sample of massive stars are too low to be compatible with SGXBs.

However, a subclass of accreting sources associated with supergiant stars, the Supergiant fast X-ray transients (SFXTs) show quiescent luminosities in the range $L_X \sim 10^{32}$ – 10^{33} erg s $^{-1}$, consistent with those of our five stars, while exhibiting flares lasting less than 1 d and reaching up to $L_X \sim 10^{36}$ erg s $^{-1}$ (Negueruela et al. 2006). The physical origin of the energetic flares is still not clear, it can be either due to the accretion of clumps from the supergiant wind or to some gating mechanism acting close to the compact accreting object. The X-ray light curves of the only source possibly associated with an early supergiant counterpart (Source #3) does not show any flaring activity characteristic of SFXTs. However, the wide range of inactivity duty cycles displayed by SFXTs (Romano et al. 2014) does not allow us to exclude an SFXT nature for this particular source.

Likewise, none of the five sources reported in this paper may qualify as an HMXBs undergoing Roche lobe overflow which usually exhibit relatively steady X-ray luminosities of the order of $L_X \sim 10^{36}$ – 10^{38} erg s $^{-1}$.

The third possible explanation for hard X-ray emission in high-mass stars is the colliding-wind binary interpretation. In this scenario, opposing winds generated in two massive stars collide producing a hot shock that is the source of hard thermal X-rays. There are many cases reported in the literature of such systems (Mauerhan et al. 2010), where WR + O stars are the most frequent association. X-ray luminosities are in the 10^{32} – 10^{34} erg s $^{-1}$ range, i.e. compatible with the X-ray luminosities observed in Source #2 and Source #3. Although in our spectra, we did not detect any additional spectral lines hinting at the presence of a O companion star, the lower optical luminosity of these objects would not allow us to detect the OB dwarf spectrum. Source #2 has very broad emission lines, associated with a very fast wind. It could also be that these emission lines are blended with a second WR star, which would not be resolved given the available resolution.

Finally, γ -Cas analogues constitute a distinct class of hard X-ray emitting Be stars (Smith, Lopes de Oliveira & Motch 2015). Confined into a narrow range of spectral types ranging from B0e to B1.5e with dwarf or giant luminosity classes, their X-ray emission appears essentially thermal with temperatures larger than 10 keV

and luminosities of a few 10^{32} erg s $^{-1}$. Both X-ray temperatures and luminosities are at variance with those displayed by normal Be stars. The origin of the X-ray emission in these objects is debated, it can either be associated with accretion on to a white dwarf companion or due to magnetic interaction between the star and the inner part of the decretion disc (Smith & Robinson 1999). However, a recent analysis of the long-term optical and X-ray light curves of γ -Cas strongly favour magnetic activity as the source of the hard X-ray emission (Motch, Lopes de Oliveira & Smith 2015). The X-ray luminosity and hard thermal spectrum of Source #5 indicate that the star is a likely new γ -Cas analogue.

We conclude that the X-ray emission of sources Source #2 and Source #3 is consistent with that expected from radiative shocks in the massive winds of single WR or Ofpe stars or from a wind-colliding binary. The supergiant Source #3 may also qualify as an SFXT in quiescence and the giant Be Source #5 is consistent with the class of γ -Cas analogues.

Source #1 and Source #4 were classified as M2I stars based on the IR spectra taken at the WHT of 2MASSJ 17434750–2923098 and 2MASSJ 18521006+0012073, respectively. RSG stars are descendants of OB stars that went through episodes of strong mass-loss during their evolution on the giant branch. Although so far no RSG has been confirmed in X-rays, Sct X-1 has been suggested as a possible HMXBs with an RSG companion (Kaplan et al. 2007). This system has been classified as a likely symbiotic binary. Symbiotic binaries are wide binaries in which a white dwarf or a neutron star accretes matter from the wind of a companion red giant star (note that Sct X-1 may have either a late giant or a supergiant luminosity class). They have soft X-ray spectra, and show optical emission line spectra. Recent studies, based on *Swift*/XRT observations, have nevertheless shown that this class of objects can also have hard X-ray spectra (Luna et al. 2013). Although we did not detect any emission line in the infrared spectra of Source #1 and Source #4 which would rule out a possible symbiotic nature of the source, there are a few symbiotic binaries lacking emission lines (Munari & Zwitter 2002; Hynes et al. 2014). The nature of the X-ray emission of Source #1 and Source #4 remains unclear. Although they could belong to the class of HMXB with a late supergiant donor stars, it is more likely that 2MASSJ 17434750–2923098 and 2MASS 18521006+0012073 are spurious infrared identifications of Source #1 and Source #4.

6.2 The nature of the hard X-ray sources

We found 690 3XMM-2MASS-GLIMPSE unique associations with reliable X-ray parameters which allowed us to discern between soft and hard X-ray sources. Making use of SIMBAD and Vizier, we compiled the list of previously classified objects (see Section 2.3). The fraction of identified sources in the soft and hard X-ray bands are similar (18 versus 16%). In Table 6, we list the number of classified X-ray sources per class of object. Soft X-ray emitters are dominated by stars with spectral types O–M, representing about 90 per cent of identified soft X-ray sources. Hard X-ray sources are dominated by HMXBs, 41 per cent of the classified hard X-ray sources. Nevertheless, the population of WR and O-B stars being discovered in the hard X-ray band is constantly increasing. In this study, we add three more sources to this new population (see Fig. 11). About 81 per cent of the identified hard X-ray sources are high-mass stars either single or in binary systems (WR+Be+HMXB+O/B from Table 6).

Table 6. Statistics of source type.

	Total	WR	Be	HMXB	LMXB	Nova	O/B	A–M	AGN	Unid
Hard	173	5	4	11	0	1	2	3	1	146
		3%	2%	6%		1%	1%	2%	1%	84%
Soft	517	7	0	0	1	0	30	55	0	424
		1%	0%	0%	0	0%	6%	11%	0%	82%
All	690	12	4	11	1	1	32	58	1	570
		2%	<1%	2%	<1%	<1%	5%	8%	<1%	83%

Notes. The table shows the fraction of each type of source among a sample of 640 X-ray sources with infrared counterparts. The cross-match procedure and the selection criteria applied to this sources are presented in Sections 2.2 and 2.3.

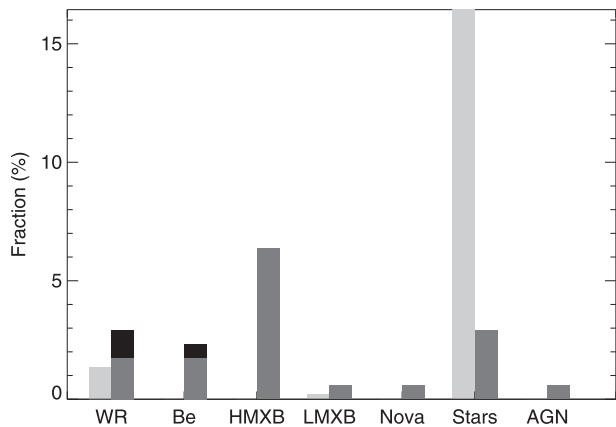


Figure 11. Fraction of soft sources (light grey) and hard sources (grey) per object type. In black, we show the position of the three X-ray sources for which we give a classification in this study.

However, the nature of six hard sources identified from the literature remains unclear. Source 3XMM J182833.7–103702 was classified as an LMXB due to the occurrence of type I X-ray bursts (Cornelisse et al. 2002). The X-ray burst showed low brightness, and furthermore it did not show a clear exponential cooling decay as can be seen from their fig. 1. Since so far the spectral type of the secondary star is not confirmed we still consider this source as an LMXB candidate (note that this is not the soft LMXB presented in Table 6). Sources 3XMM J155033.7–540916 and 3XMM J183255.1–100741 have been classified as AGB candidates and 3XMM J184841.0–023929 as a YSO candidate by Robitaille et al. (2008). Sources 3XMM J182746.3–120605 and 3XMM J182814.3–103728 have been classified as candidate HMXBs by (Motch et al. 2010, XGPS 10 and XGPS 15, respectively). The hard sample source 3XMM J182746.3–120605 is the same as XGPS-10 in Motch et al. (2010). We note that the position used for XGPS-10 in the latter work (RA = 18:27:45.49, Dec. = –12:06:06.7) was derived from an early *XMM–Newton* reduction pipeline in 2001 and is very significantly offset by 12.2 arcsec with respect to that now provided by the 3XMM catalogue. Accordingly, the faint possible candidate deemed as uncertain by Motch et al. (2010) cannot be the actual counterpart. Our work shows that XGPS-10 is in fact identified with the nearby bright $K=11.94$ infrared source. To conclude, since the nature of these six sources is still not confirmed, we prefer to leave them as unidentified (i.e. among the 146 Hard Unid in Table 6), meaning that a confirmation of their nature is needed.

Finally, three stars classified as active coronae have hard X-ray spectra. These three stars have all G spectral type. Although active

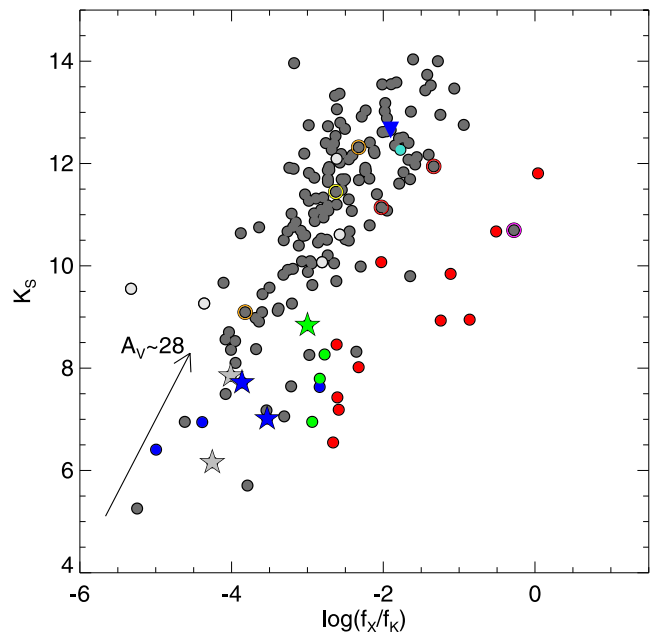


Figure 12. Infrared K_s magnitude versus X-ray-to-infrared flux ratio (in the 2–12 keV band) for hard X-ray sources. Plotted with filled circles are confirmed stars (2 B and 3 G stars, light grey), HMXBs (red), Be stars (green), and WR stars (blue). The only AGN from the sample is shown as a blue filled upside down triangle and a Nova as a turquoise filled circle. Unidentified sources are shown in dark grey, surrounded by a coloured ring when a candidate classification of the source is available: candidate HMXBs (red), candidate YSO (yellow), candidate AGB stars (orange), candidate LMXB (magenta). Targets observed at the telescope are highlighted with a star symbol colour coded according to their classification. The effect of extinction assuming a population of hard X-ray massive stars (model 3 in Section 2.3) is shown with an arrow.

stellar coronae have typically soft X-ray spectra, many BY Draconis and RS CVn binaries, i.e. main sequence and evolved binaries, have been detected in hard X-rays (e.g. II Peg; Osten et al. 2007). The three G stars in this sample could belong to these types of objects.

We show the K_s magnitude versus X-ray-to-infrared flux ratio $\log(f_x/f_{K_s})$ for hard sources in Fig. 12, highlighting the position of the different types of objects found (HMXBs, WR, Be stars and late-type stars). In our hard X-ray source sample, WR stars dominate at X-ray-to-infrared flux ratios $\log(f_x/f_{K_s}) < -2.6$, Be stars cover a very narrow range of values (although there are only a few of these systems), with mean $\log(f_x/f_{K_s}) \sim -2.6$, and HMXB dominate at higher values, $\log(f_x/f_{K_s}) > -2.7$. It should be stressed that the sources we selected for identification at the telescope in our pilot

Table 7. HMXBs and Be stars identified from the literature.

Source name	Sp type	$\log(f_X/f_{K_S})$	HR3	Ks	Note
HD 119682	B0.5Ve	-2.56	-0.21	6.95	γ -Cas analogue
SS 397	B0.5Ve	-2.60	+0.08	8.27	γ -Cas analogue
NGC 6649 WL 9	B1-1.5IIIe	-2.73	+0.15	7.79	γ -Cas analogue
IGR J16318-4848	SgB[e]	-2.60	+0.89	7.19	Supergiant X-ray binary
EXO 1722-363	B0-1Ia	-0.53	+0.96	10.67	Wind fed Sg accreting neutron star
Sct X-1	late Sg	-2.67	+0.92	6.55	Supergiant X-ray binary
AX J1910.7+0917	B	+0.04	+0.82	11.81	Early B-type supergiant star
AX J1749.2-2725 ^a	B3	-2.04	0.976	10.07	Wind-fed accreting neutron stars
IGR J16465-4507	O9.5Ia	-1.08	+0.51	9.84	SFXT
XTE J1739-302	O8.5Iab	-2.55	+0.62	7.43	SFXT
IGR J17544-2619	O9Ib	-2.26	+0.50	8.02	SFXT
IGR J18410-0535	B1Ib	-1.26	+0.93	8.93	SFXT
IGR J18450-0435	O9Ia	-0.82	+0.59	8.95	SFXT
IGR J18483-0311	B0.5Ia	-2.59	+0.82	8.46	SFXT

Notes. ^aThe infrared counterpart of AX J1749.2-2725 from which a spectral type B was determined has infrared magnitudes fainter than those we determine in this paper, implying the infrared counterpart is different. Kaur et al. (2010) derived the X-ray position from *XMM* and *Chandra* observations and infrared imaging and spectroscopy was carried out at the NTT, e.g. with a better resolution than 2MASS. We note that our identification of the true counterpart of the source might be wrong.

study are in no way representative of the entire set of pre-selected hard X-ray sources. First, we selected the brightest infrared sources for reasons of efficiency. Since our X-ray sample is flux-limited, this implied selecting sources at the low end of the X-ray-to-infrared flux ratio distribution. In addition, as shown in Fig. 3, our pilot sample lies among the most reddened or intrinsically red stars. This is due in part to the presence of two possible M2I interlopers and to the two WR stars. Finally, due to the location of the WHT, we could only survey the Northern part of the Galactic plane covered by GLIMPSE.

More information on the likely source content of the hard sample can be derived from identifications made through archival catalogues and from the literature. Table 7 lists HMXBs and γ -Cas analogues present in our sample.

We found that the various classes of sources were best separated in a 3D space which axis are an infrared colour (giving information on both intrinsic colours and amount of reddening) HR3 (which is the best-defined proxy of the X-ray spectral hardness) and the X-ray-to-infrared flux ratio (which provides information on the emission mechanism). The top panel in Fig. 13 shows the distribution of the hard sample in this 3D space, while introducing an IR magnitude allow us to sort out identified sources from the rest of the unidentified population (see the bottom panel in Fig. 13).

The group of four γ -Cas analogues (three previously identified) share similar X-ray and infrared colours and exhibit very comparable average X-ray-to-infrared flux ratios. As illustrated in the two panels in Fig. 13, many hard sources have properties similar to those of γ -Cas analogues, albeit with fainter magnitudes and expected larger distances and may indeed be good candidates for belonging to this particular class.

Very few active coronae have hard enough X-ray spectra to qualify as a hard X-ray source. However, several of the hard sources with $\text{HR3} \leq 0.6$, $\log(f_X/f_{K_S})$ in the range of -2 to -3 and no infrared excess could still be identified with extreme active coronae.

Compared to γ -Cas analogues, WR stars display on average softer X-ray spectra. Consequently, several of the WR stars identified in the literature actually failed to qualify as hard sources due to their too soft HR4, although their HR3 were fulfilling our conditions. It is thus unlikely that many WR stars appear in our selection

of hard sources with $\text{HR3} \leq 0.2$. However, four WR stars, two identified in the literature and two from our work, are found among our sample of hard sources with $\text{HR3} \geq 0.2$. Accordingly, we expect to discover new X-ray selected WR stars in the region comprising the hardest X-ray sources with low to medium X-ray-to-infrared flux ratios. We note that the WRs in our sample fall in Mauerhan et al. (2010) best selection areas in the (K_s -8.0 μm) colour (see their Fig. 8.)

The top panel in Fig. 13 shows the presence of several hard sources in the region bounded by $\text{HR3} \geq 0.4$, $\log(f_X/f_{K_S}) \geq -3$ and low-to-high infrared excess. This area is populated by supergiant X-ray binaries and prospects are therefore relatively good that we find new massive X-ray binaries in this sample. Their relatively modest X-ray-to-infrared flux ratios would rather suggest SFXTs or classical Be/X-ray transients in the close to quiescence state. We note that among our relatively small sample of HMXBs SFXTs seem to display bluer IR colours.

The nature of the population of faint ($K_s \geq 11$) sources with $\log(f_X/f_{K_S})$ in the range of -2 to -1 and $\text{HR3} \leq 0.5$ (yellow spots in Fig. 13) remains essentially unconstrained since only one identified source shares these properties, an AGN. Our identified AGN has $\log(f_X/f_{K_S}) = -1.90$, $\text{HR3} = 0.60$, $K_s = 12.65$ and $H - 4.5 \mu = 1.88$. We determined the total galactic extinction in the line of sight using the Schlegel maps (Schlegel, Finkbeiner & Davis 1998), and found no relation between the measured HR2 or HR3 and the total N_H for hard sources with $K_s \geq 11$ and $\log(f_X/f_{K_S}) \geq -2.5$. The nature of this group of faint sources is thus not dominated by a population of background AGN. Likewise, the significantly higher X-ray-to-infrared flux ratio displayed by these faint sources compared to brighter ones suggests that they do not represent a reddened and remote population of sources identified at shorter distances.

7 CONCLUSIONS

We presented a study which aims at finding hard X-ray high-mass stars with low- to intermediate- X-ray luminosity. For that purpose, we cross-correlated the 3XMM-DR4 catalogue with the 2MASS and GLIMPSE catalogues. We pre-selected 173 hard X-ray sources

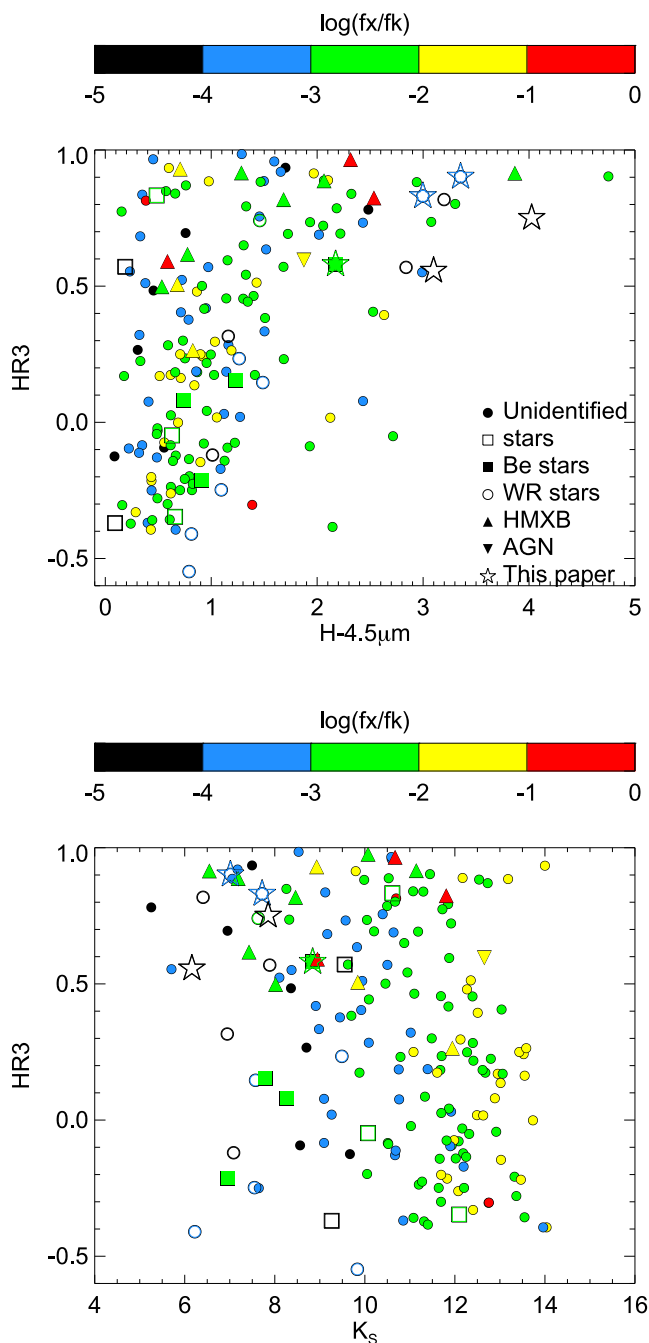


Figure 13. Colours of hard X-ray sources. In both figures, symbols are colour coded according to the ratio of X-ray-to-infrared fluxes. Unclassified sources are shown as filled circles, WRs as open circles (we also included soft WRs in these two plots), HMXBs as triangles, Be stars as filled squares and other stars with open squares. The position of the only AGN is shown with an upside down triangle. Targets observed in this study are highlighted with a five pointed star symbol.

with bright infrared counterparts and with harder X-ray spectra (HR) than expected for a normal stellar corona. Among these 173 hard X-ray sources, 25 were previously classified: 3 WRs, 3 Be stars, 11 HMXBs, 1 LMXB, 1 Nova, 5 stars and 1 AGN. In this pilot study, we carried out infrared spectroscopy of five new high-mass star candidates. We derived spectral types, and stellar parameters for these systems. We confirmed three sources as being high-mass hard X-ray stars with spectral types WN7-8h, Ofpe/WN9 and Be

and with X-ray luminosities in the range $\sim 10^{32}$ – 10^{33} erg s $^{-1}$ (0.2–12 keV). One source is compatible with a colliding-wind binary, another source is compatible with both a colliding-wind binary and an SFXT and one source is a γ -Cas analogue candidate. We classified two 2MASS sources as supergiant stars, both with an M2 I spectral type, and concluded that they are likely not the true counterpart of the X-ray sources, whose nature is still unknown, although they could also belong to the class of HMXBs with a late supergiant star. Finally, the distribution of hard X-ray sources in the parameter space made of X-ray HR, infrared colours and X-ray-to-infrared flux ratio suggests that many of the unidentified sources are new γ -Cas analogues, WRs and low L_X HMXBs. However, the nature of the X-ray population appearing at $K_s \geq 11$ and exhibiting average X-ray-to-infrared flux ratios remains unconstrained.

ACKNOWLEDGEMENTS

This work is based on service observations made with the WHT operated on the island of La Palma by the Isaac Newton Group in the Spanish Observatorio del Roque de los Muchachos of the Instituto de Astrofísica de Canarias. We would like to thank our referee I. Negueruela for his useful comments which significantly helped improving the quality of this work. We also thank P. A. Crowther and C. K. Rosslowe for sharing with us their new calibrated infrared WR absolute magnitudes. We acknowledge financial support from the ARCHES project (7th Framework of the European Union, no. 313146). FJC acknowledges financial support from the Spanish Ministerio de Economía y Competitividad under project AYA2012-31447. This publication makes use of data products from the 2MASS, which is a joint project of the University of Massachusetts and the Infrared Processing and Analysis Center/California Institute of Technology, funded by the National Aeronautics and Space Administration and the National Science Foundation. This work is based in part on observations made with the *Spitzer* Space Telescope, which is operated by the Jet Propulsion Laboratory, California Institute of Technology under a contract with NASA. This research has made use of NASA's Astrophysics Data System. This research has made use of the SIMBAD and VizieR data bases, operated at CDS, Strasbourg, France. Based on spectral-fitting results from the *XMM-Newton* spectral-fit data base, an ESA PRODEX funded project, based in turn on observations obtained with *XMM-Newton*, an ESA science mission with instruments and contributions directly funded by ESA Member States and NASA.

REFERENCES

- Anderson L. D., Bania T. M., Jackson J. M., Clemens D. P., Heyer M., Simon R., Shah R. Y., Rathborne J. M., 2009, *ApJS*, 181, 255
 Anderson G. E. et al., 2011, *ApJ*, 727, 105
 Becker R. H., White R. L., Helfand D. J., Zoonematkermani S., 1994, *ApJS*, 91, 347
 Benjamin R. A. et al., 2003, *PASP*, 115, 953
 Blum R. D., Daminieli A., Conti P. S., 2001, *AJ*, 121, 3149
 Bonnarel F. et al., 2000, *A&AS*, 143, 33
 Cardelli J. A., Clayton G. C., Mathis J. S., 1989, *ApJ*, 345, 245
 Carey S. J. et al., 2009, *PASP*, 121, 76
 Castelli F., Kurucz R. L., 2004, preprint ([arXiv:astro-ph/0405087](https://arxiv.org/abs/astro-ph/0405087))
 Chaty S., 2011, in Schmidtobreick L., Schreiber M. R., Tappert C., eds, *ASP Conf. Ser. Vol. 447, Evolution of Compact Binaries*. Astron. Soc. Pac., San Francisco, p. 29
 Churchwell E. et al., 2006, *ApJ*, 649, 759
 Churchwell E. et al., 2009, *PASP*, 121, 213

- Clark J. S., Steele I. A., 2000, *A&AS*, 141, 65
- Cornelisse R. et al., 2002, *A&A*, 392, 885
- Corral A., Georgantopoulos I., Rosen S., Watson M. G., Page K., Stewart G. C., 2015, *A&A*, 576A, 61
- Covey K. R. et al., 2007, *AJ*, 134, 2398
- Crowther P. A., Hadfield L. J., Clark J. S., Negueruela I., Vacca W. D., 2006, *MNRAS*, 372, 1407
- Cutri R. M. et al., 2003, *VizieR Online Data Catalog*, 2246, 0
- Cutri R. M. et al., 2012, *VizieR Online Data Catalog*, 2311, 0
- Deharveng L. et al., 2010, *A&A*, 523, A6
- Deharveng L. et al., 2012, *A&A*, 546, A74
- Dempsey R. C., Linsky J. L., Schmitt J. H. M. M., Fleming T. A., 1993, *ApJ*, 413, 333
- den Herder J. W. et al., 2001, *A&A*, 365, L7
- Ebisawa K. et al., 2005, *ApJ*, 635, 214
- Egan M. P. et al., 2003, *VizieR Online Data Catalog*, 5114, 0
- Figer D. F., McLean I. S., Najarro F., 1997, *ApJ*, 486, 420
- Förster Schreiber N. M., 2000, *AJ*, 120, 2089
- Gagné M., Oksala M. E., Cohen D. H., Tonnesen S. K., ud-Doula A., Owocki S. P., Townsend R. H. D., MacFarlane J. J., 2005, *ApJ*, 628, 986
- Gagné M. et al., 2011, *ApJS*, 194, 4
- Gilfanov M., 2004, *MNRAS*, 349, 146
- Grimm H.-J., Gilfanov M., Sunyaev R., 2002, *A&A*, 391, 923
- Güdel M., Guinan E. F., Skinner S. L., 1997, *ApJ*, 483, 947
- Hamann W.-R., Gräfener G., 2004, *A&A*, 427, 697
- Hands A. D. P., Warwick R. S., Watson M. G., Helfand D. J., 2004, *MNRAS*, 351, 31
- Hanson M. M., Rieke G. H., Luhman K. L., 1998, *AJ*, 116, 1915
- Hanson M. M., Kudritzki R.-P., Kenworthy M. A., Puls J., Tokunaga A. T., 2005, *ApJS*, 161, 154
- Helfand D. J., Becker R. H., White R. L., Fallon A., Tuttle S., 2006, *AJ*, 131, 2525
- Hoare M. G. et al., 2012, *PASP*, 124, 939
- Hofner P., Delgado H., Whitney B., Churchwell E., Linz H., 2002, *ApJ*, 579, L95
- Hong J. S., van den Berg M., Grindlay J. E., Laycock S., 2009, *ApJ*, 706, 223
- Horne K., 1986, *PASP*, 98, 609
- Hynes R. I. et al., 2014, *ApJ*, 780, 11
- Indebetouw R. et al., 2005, *ApJ*, 619, 931
- Jansen F. et al., 2001, *A&A*, 365, L1
- Kaplan D. L., Levine A. M., Chakrabarty D., Morgan E. H., Erb D. K., Gaensler B. M., Moon D.-S., Cameron P. B., 2007, *ApJ*, 661, 437
- Kaur R., Wijnands R., Paul B., Patruno A., Degenaar N., 2010, *MNRAS*, 402, 2388
- Kobulnicky H. A., Babler B. L., Alexander M. J., Meade M. R., Whitney B. A., Churchwell E. B., 2013, *ApJS*, 207, 9
- Levesque E. M., Massey P., Olsen K. A. G., Plez B., Josselin E., Maeder A., Meynet G., 2005, *ApJ*, 628, 973
- Lopes de Oliveira R., 2007, PhD thesis, Univ. São Paulo
- Lucy L. B., White R. L., 1980, *ApJ*, 241, 300
- Luna G. J. M., Sokolowski J. L., Mukai K., Nelson T., 2013, *A&A*, 559, A6
- Marigo P., Girardi L., Bressan A., Groenewegen M. A. T., Silva L., Granato G. L., 2008, *A&A*, 482, 883
- Marshall D. J., Robin A. C., Reylé C., Schultheis M., Picaud S., 2006, *A&A*, 453, 635
- Martins F., Plez B., 2006, *A&A*, 457, 637
- Mateos S., Saxton R. D., Read A. M., Sembay S., 2009, *A&A*, 496, 879
- Mauerhan J. C., Muno M. P., Morris M. R., Bauer F. E., Nishiyama S., Nagata T., 2009, *ApJ*, 703, 30
- Mauerhan J. C., Muno M. P., Morris M. R., Stolovy S. R., Cotera A., 2010, *ApJ*, 710, 706
- Messineo M., Zhu Q., Ivanov V. D., Figer D. F., Davies B., Menten K. M., Kudritzki R. P., Chen C.-H. R., 2014, *A&A*, 571, A43
- Meynet G., Maeder A., 2000, *A&A*, 361, 101
- Monet D. G. et al., 2003, *AJ*, 125, 984
- Morris P. W., Eenens P. R. J., Hanson M. M., Conti P. S., Blum R. D., 1996, *ApJ*, 470, 597
- Motch C., Guillout P., Haberl F., Pakull M., Pietsch W., Reinsch K., 1997, *A&A*, 318, 111
- Motch C., Herent O., Guillout P., 2003, *Astron. Nachr.*, 324, 61
- Motch C., Lopes de Oliveira R., Negueruela I., Haberl F., Janot-Pacheco E., 2007, in Okazaki A. T., Owocki S. P., Stefl S., eds, *ASP Conf. Ser. Vol. 361, Active OB-Stars: Laboratories for Stellar and Circumstellar Physics*. Astron. Soc. Pac., San Francisco, p. 117
- Motch C. et al., 2010, *A&A*, 523, A92
- Motch C., Lopes de Oliveira R., Smith M. A., 2015, preprint ([arXiv:1504.01105](https://arxiv.org/abs/1504.01105))
- Munari U., Zwitter T., 2002, *A&A*, 383, 188
- Muno M. P. et al., 2009, *ApJS*, 181, 110
- Nebot Gómez-Morán A. et al., 2013, *A&A*, 553, A12
- Negueruela I., Smith D. M., Reig P., Chaty S., Torrejón J. M., 2006, in Wilson A., ed., *EESA SP-604: The X-ray Universe 2005*. ESA, Noordwijk, p. 165
- Negueruela I., González-Fernández C., Marco A., Clark J. S., Martínez-Núñez S., 2010, *A&A*, 513, A74
- Negueruela I., González-Fernández C., Marco A., Clark J. S., 2011, *A&A*, 528, A59
- Nesterov V. V., Kuzmin A. V., Ashimbaeva N. T., Volchkov A. A., Röser S., Bastian U., 1995, *A&AS*, 110, 367
- Ochsenbein F., Bauer P., Marcout J., 2000, *A&AS*, 143, 23
- Oskinoval L. M., Hamann W.-R., Feldmeier A., Ignace R., Chu Y.-H., 2009, *ApJ*, 693, L44
- Osten R. A., Drake S., Tueller J., Cummings J., Perri M., Moretti A., Covino S., 2007, *ApJ*, 654, 1052
- Peretto N., Fuller G. A., 2009, *A&A*, 505, 405
- Pfahl E., Rappaport S., Podsiadlowski P., 2002, *ApJ*, 571, L37
- Pineau F.-X., Motch C., Carrera F., Della Ceca R., Derrière S., Michel L., Schwobe A., Watson M. G., 2011, *A&A*, 527, A126
- Predehl P., Schmitt J. H. M. M., 1995, *A&A*, 293, 889
- Raguzova N. V., 2001, *A&A*, 367, 848
- Revnivtsev M., Sazonov S., Churazov E., Forman W., Vikhlinin A., Sunyaev R., 2009, *Nature*, 458, 1142
- Robitaille T. P. et al., 2008, *AJ*, 136, 2413
- Romano P., Ducci L., Mangano V., Esposito P., Bozzo E., Vercellone S., 2014, *A&A*, 568, A55
- Rosslowe C. K., Crowther P. A., 2015, *MNRAS*, 447, 2322
- Sanna A. et al., 2014, *ApJ*, 781, 108
- Sazonov S., Revnivtsev M., Gilfanov M., Churazov E., Sunyaev R., 2006, *A&A*, 450, 117
- Schlegel D. J., Finkbeiner D. P., Davis M., 1998, *ApJ*, 500, 525
- Schultheis M. et al., 1999, *A&A*, 349, L69
- Sguera V. et al., 2006, *ApJ*, 646, 452
- Shara M. M. et al., 2009, *AJ*, 138, 402
- Skinner S. L., Zhekov S. A., Güdel M., Schmutz W., Sokal K. R., 2010, *AJ*, 139, 825
- Skrutskie M. F. et al., 2006, *AJ*, 131, 1163
- Smith M. A., Robinson R. D., 1999, *ApJ*, 517, 866
- Smith M. A., Lopes de Oliveira R., Motch C., 2015, in Sigut A., C. J., eds, *ASP Conf. Ser. Vol. 0, Bright Emissaries*, p. 0
- Sokal K. R., Skinner S. L., Zhekov S. A., Güdel M., Schmutz W., 2010, *ApJ*, 715, 1327
- Spitzer Science C., 2009, *VizieR Online Data Catalog*, 2293, 0
- Stead J. J., Hoare M. G., 2011, *MNRAS*, 418, 2219
- Steele I. A., Clark J. S., 2001, *A&A*, 371, 643
- Strüder L. et al., 2001, *A&A*, 365, L18
- Sugizaki M., Mitsuda K., Kaneda H., Matsuzaki K., Yamauchi S., Koyama K., 2001, *ApJS*, 134, 77
- Tauris T. M., van den Heuvel E. P. J., 2006, in Lewin W. H. G., van der Klis M., eds, *Compact Stellar X-ray Sources*. Cambridge Univ. Press, Cambridge, p. 623
- Taylor M., 2011, *Astrophysics Source Code Library*, record ascl:1101.010

- Torrejón J. M., Schulz N. S., Nowak M. A., Testa P., Rodas J. J., 2013, *ApJ*, 765, 13
- Turner M. J. L. et al., 2001, *A&A*, 365, L27
- van Belle G. T. et al., 1999, *AJ*, 117, 521
- Watson M. G. et al., 2009, *A&A*, 493, 339
- White R. L., Becker R. H., Helfand D. J., 2005, *AJ*, 130, 586
- Wright E. L. et al., 2010, *AJ*, 140, 1868
- Yamaguchi H., Ueno M., Koyama K., Bamba A., Yamauchi S., 2004, *PASJ*, 56, 1059

SUPPORTING INFORMATION

Additional Supporting Information may be found in the online version of this article:

Table 2. Infrared counterparts of X-ray sources. (<http://mnras.oxfordjournals.org/lookup/suppl/doi:10.1093/mnras/stv1020/-/DC1>).

Please note: Oxford University Press are not responsible for the content or functionality of any supporting materials supplied by the authors. Any queries (other than missing material) should be directed to the corresponding author for the article.

APPENDIX A: NOTES ON B AND BE HARD X-RAY STARS

We briefly discuss the nature of the hard B and Be stars found in this study via cross-correlations with SIMBAD and our spectroscopic observations.

3XMM J134632.5–625524. The optical counterpart of 3XMM J134632.5–625524, HD 119682, was found to be a B0.5Ve star at a distance of 1.3 kpc and with X-ray luminosity $L_X \sim 10^{32}$ erg s⁻¹, belonging to the class of γ -Cas analogues (see Torrejón et al. 2013, and references therein). It is a blue straggler belonging to the open cluster NGC 5281 at a distance of 1.3 kpc.

3XMM J181046.7–194421. This X-ray source is likely associated with HD 312792 which was classified as B5 by Nesterov et al. (1995). Visual inspection of the optical spectra used for stellar classification was not possible. No estimates for the stellar luminosity class and distance to the star were found in the literature.

3XMM J182746.3–120605. aka XGPS-I J182745–120606 is identified with XGPS-10 (Motch et al. 2010). We note that the position used for XGPS-10 in the latter work (RA = 18:27:45.49, Dec. = -12:06:06.7) was derived from an early *XMM-Newton* reduction pipeline in 2001 and is very significantly offset by 12.2 arcsec with respect to that now provided by the 3XMM

catalogue. Accordingly, the faint possible candidate deemed as uncertain by Motch et al. (2010) cannot be the actual counterpart. Our work shows that XGPS-10 is identified with the nearby bright K=11.94 infrared source.

3XMM J182814.3–103728. Based on the optical spectrum, which revealed H α emission and Paschen absorption lines, Motch et al. (2010) classified the source as a possible B star (source XGPS-15). Although the authors noted the possibility of the optical source being an interloper. At a distance of about 10 kpc, consistent with the strong extinction observed for this source, its X-ray luminosity is $\sim 2.4 \times 10^{34}$ erg s⁻¹. The source was classified by Motch et al. (2010) as an HMXB candidate, with a giant or supergiant star as secondary star. As for the case above, if the optical counterpart is a blue supergiant the source would not belong to the class of Be stars.

3XMM J182828.0–102401. A spectrum taken for the optical counterpart USNO-A2.0 0750-13261865 revealed a B3 spectral type (Motch et al. 2010) lacking emission lines. No luminosity class and distance values are available in the literature.

3XMM J183327.7–103524. Optical identification of the X-ray source 3XMM J183327.7–103524 was first presented by Motch, Herent & Guilloit (2003). The optical spectrum of SS 397 revealed a B0 V star. Nebot Gómez-Morán et al. (2013) estimated a distance to the source of 1.5 kpc and an X-ray luminosity of $L_X = 4.4 \times 10^{32}$ erg s⁻¹, and suggested the source to be a likely γ -Cas analogue.

3XMM J183328.3–102408. Based on spectroscopic observations of the optical counterpart USNO0750-13549725 C, Nebot Gómez-Morán et al. (2013) classified the source as a B1–1.5 IIIe star. They estimated a distance to the star of 1.7 kpc, a value consistent with that to the cluster NGC6649. USNO0750-13549725 C is the brightest star in the cluster and it is a blue straggler. It is X-ray luminosity is $L_X = 6 \times 10^{32}$ erg s⁻¹. The source belongs to the γ -Cas analogue class.

3XMM J190144.5+045914. We classified the source in this study as a Be star, at a distance in the range 1–1.8 kpc and a luminosity of $L_X = 0.9$ to 3.0×10^{32} erg s⁻¹. This source belongs to the class of γ -Cas analogues.

Out of the eight hard B stars presented in this section, two are Be/X-ray high-mass binary candidates with X-ray luminosities $L_X \sim 10^{34}$ erg s⁻¹ (both with a giant or supergiant secondary star), four are γ -Cas analogues with $L_X \sim 10^{32}$ erg s⁻¹, and two are B stars with no emission lines detected so far.

This paper has been typeset from a \LaTeX file prepared by the author.